11

Rates of flow and patterns of fluid circulation

Andrew T. Fisher

11.1 Significance of fluid circulation rates and patterns

The rates and patterns of fluid circulation in seafloor hydrothermal systems control the efficiency of lithospheric heat extraction, the nature of fluid–rock interaction, and the extent of seafloor and sub-seafloor biospheres supported by fluid, energy, and solute fluxes. It has been challenging to determine the patterns and rates of fluid flow within seafloor hydrothermal systems for several reasons. Active systems are remote and measurements are often difficult to make. Although newly developed tools have led to important advances in *in situ* characterization (Chapter 8), considerable challenges remain in determining where and how quickly fluids move through the sub-seafloor environment. Fossil systems provide an integrated record of fluid flow (Chapter 9), but system heterogeneity and overprinting of multiple generations of activity make quantitative interpretation difficult. Exposures are limited within both active and fossil systems, with the former often restricted to widely spaced or isolated boreholes and seafloor outcrops, and the latter comprising mainly ophiolites and rare seafloor exposures (for example, along fracture zones or rifts, e.g. Karson, 2002). Fluid flow within seafloor hydrothermal systems is transient on a range of time scales, and some of these systems operate over lateral and vertical distances of kilometers or more. Additional complexities arise due to the scaling of rock properties within heterogeneous, fractured crust (Chapter 7). A more subtle difficulty is the influence of assumptions and ideas that became embedded in the literature at an early stage of research. Even after some of these ideas have been found to conflict with observations, they continue to influence interpretations.

In this chapter, rates of fluid flow in hydrothermal systems, the lateral extent of circulation, preferred directions of fluid flow, and the "shapes" of fluid pathways are discussed. Techniques applied to resolve these parameters include use of thermal and chemical tracers, seafloor and borehole observations, and coupled modeling. Considerably more is known about apparent rates of fluid flow than is known about overall patterns of fluid circulation, but even estimates of rates should be viewed with caution because estimates are generally based on fundamental assumptions regarding the primary direction of flow, nature of

Hydrogeology of the Oceanic Lithosphere, eds. E. E. Davis and H. Elderfield. Published by Cambridge University Press.

the flow pathways, and other critical parameters. The delineation of fluid flow pathways remains a topic of intense debate within land-based hydrogeologic systems, where there is often extensive access to data and samples; the paucity of available seafloor data is bound to result in considerable uncertainty. Although the focus of this book is on ridge flank hydrothermal systems, limited observations and inferences from studies of ridge crest systems are also presented because crustal properties acquired at the ridge (Chapters 3, 9, and 15) are likely to have continued influence as the seafloor evolves (Chapter 5).

11.2 Rates of fluid circulation

11.2.1 Flow-rate concepts and nomenclature

Researchers concerned with global thermal and geochemical budgets often refer to quantities of volume flow [L^3/T] or mass flow [M/T], but these are difficult to determine by direct measurement, even at known exit points of hydrothermal venting (Converse *et al*., 1980; Schultz *et al*., 1992). Instead, estimates of volume flow from these systems are often made at a larger scale (that of the vent field, ridge segment, or global ocean) based on a tracer such as heat or a conservative solute (e.g. Baker *et al*., 1996; Elderfield and Schultz, 1996; Mottl *et al*., 1998).

Rates of fluid flow in hydrogeologic systems are often discussed in terms of either fluid velocity ($\boldsymbol{u}$) or volume discharge per area ($\boldsymbol{q}$), both of which have dimensions of [L/T]. In this text we use the term "flux" to describe the latter, although in the hydrogeologic literature the terms "specific discharge" or "Darcy velocity" are commonly used. Average fluid velocity relates to flux through the effective porosity, $\boldsymbol{u} = \boldsymbol{q}/n_e$, where n_e is the volume fraction of rock occupied by pores or fractures that contribute significantly to fluid flow. As a practical matter, determining the effective porosity independent of flux and velocity is difficult. The average velocity is a lower limit to the local particle velocity because hydrogeologic flow paths tend to be tortuous. In fact, it is not possible to determine an upper limit on particle velocities within hydrothermal systems because the rate of internal mixing (that not contributing to net flow through the system) cannot be measured once it becomes sufficiently rapid so as to homogenize the fluid in storage.

A reservoir is a region within which fluid, energy, or solutes are stored. Distinct reservoirs (i.e. for fluid and heat) may coincide in location and shape, or they may be physically separated. Reservoirs may change in location and shape with time or may be entirely conceptual. Even if it is not possible to define reservoir boundaries, the reservoir concept provides a framework for discussion of water/rock interaction (i.e. the reservoir is the place where emerging sub-surface water acquires a characteristic chemistry, etc.).

Fluid flow rate and reservoir concepts can be combined through calculation of a residence time, t_r. The residence time can be calculated on the basis of fluid reservoir size and mass (or volume) rate of fluid flow: t_r = mass storage/mass flow rate (or volume storage/volume flow rate) or on the basis of energy, t_r = energy storage/energy flow rate. Of the two fluid flow options, the mass calculation makes more sense for high-temperature hydrothermal

systems because of large differences in fluid density associated with changes in pressure and enthalpy. The residence time concept strictly applies only to systems at dynamic steady state, where there is no change in flow rate or the quantity in storage. Under these conditions, for a system that is perfectly well mixed (every particle has an equal probability of appearing anywhere in the reservoir at any time), the residence time represents the average amount of time that each particle will spend in the reservoir. For an idealized "single-pass" system, in which fluid moves as a plug from one end to the other, the residence time is the same as the travel time calculated on the basis of average fluid velocity. For more complex systems, in which there is considerable recirculation, mixing, or exchange between reservoirs, particle residence times could be considerably different from those calculated under the assumption of single-pass, plug flow.

Diffusion and dispersion are discussed in this chapter with regard to solute transport. Diffusion is a process by which matter is transported from one part of a system to another through random molecular (Brownian) motion, with net transport occurring from areas of high concentration to areas of low concentration (Crank, 1975). Solutes have a coefficient of diffusion in pure water, a term that is independent of concentration and fluid flow rate but depends on temperature, species, and interaction between species. The effective diffusion coefficient within a porous medium is usually lower than the value in pure water because diffusion is considerably more rapid within the fluid of a pore network than through solid matrix material, and the pore network generally occupies a small fraction of the rock volume. Hydrodynamic dispersion comprises a combination of diffusion and mechanical dispersion, a process that results from differences in solute transport rates within and between pore channels. Rather than being constant like the diffusion coefficient, mechanical dispersion varies with fluid velocity, as described with a coefficient called dispersivity. Dispersivity is known to vary with measurement length (Neuman, 1990; Gelhar *et al.*, 1992); its value must be determined at the scale of interest.

11.2.2 Estimating vertical fluxes

One method for estimating vertical fluid fluxes in groundwater systems was introduced by Bredehoeft and Papadopulos (1965). A horizontal confining layer (a geological unit having a permeability that is low relative to that of surrounding materials) is bounded at the top and bottom by interfaces held at constant temperatures, and flow across the confining layer is entirely vertical and occurs at steady state (Fig. 11.1). The assumption of vertical flow through a sub-horizontal confining layer is generally reasonable, as fluids tend to take the shortest possible path through units having low permeability (see Section 11.3). The assumption that upper and lower boundaries have fixed temperatures is most appropriate when the flux through the confining layer is modest relative to the size of overlying and underlying reservoirs. In the case of seafloor hydrothermal systems, this model has been applied most commonly to marine sediments, bounded at the top by the ocean (essentially an infinite sink for heat), and at the base by a hydrothermal reservoir (allowing application of either a constant temperature or a constant heat flux boundary condition, as discussed

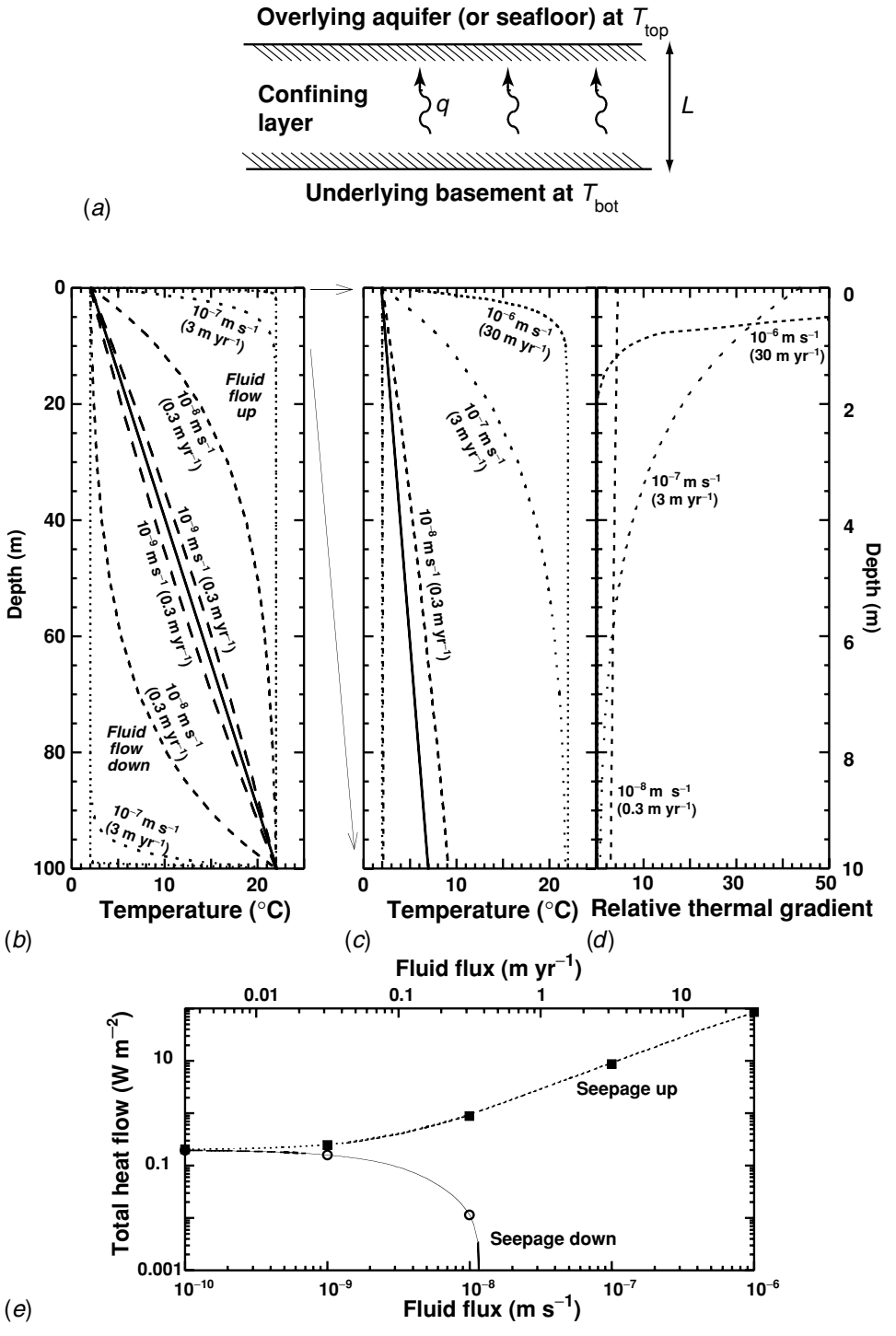
Overlying aquifer (or seafloor) at T_{top}
Confining layer
q
L
Underlying basement at T_{bot}
(a)
Depth (m)
Temperature (°C)
Fluid flow up
Fluid flow down
10^{-7} m s^{-1} (3 m yr^{-1})
10^{-8} m s^{-1} (0.3 m yr^{-1})
10^{-9} m s^{-1} (0.3 m yr^{-1})
(b)
10^{-6} m s^{-1} (30 m yr^{-1})
(c)
Relative thermal gradient
(d)
Fluid flux (m yr^{-1})
Total heat flow (W m^{-2})
Seepage up
Seepage down
Fluid flux (m s^{-1})
(e)

later). The same theory can be applied to basement layers, in principle, but it has proven difficult to determine equilibrium formation temperatures within hard rock.

For the case of constant-temperature boundaries, temperatures at depth, z, below the upper boundary may be calculated (Bredehoeft and Papadopulos, 1965) as:

$$T(z) = T_{\text{top}} + (T_{\text{bot}} - T_{\text{top}}) \left[\frac{\exp\left(\beta \frac{z}{L}\right) - 1}{\exp(\beta) - 1} \right] \tag{11.1}$$

where $\beta = (\rho_w c_w q L)/\lambda$, $\rho_w c_w$ = volumetric heat capacity of water, L = layer thickness, and λ = thermal conductivity of the fluid-saturated matrix. Example calculations illustrate several important characteristics of this solution. Imagine a sediment layer 100 m thick, with fixed temperature boundaries ($T_{\text{bot}} - T_{\text{top}} = 20\,^{\circ}\text{C}$) and a constant thermal conductivity of 1 W m^{-1} °C^{-1}. In the absence of fluid flow, conductive heat flux would be 0.2 W m^{-2} (Fig. 11.1). A vertical seepage flux in excess of $\sim 10^{-9}$ m s^{-1} (30 mm yr^{-1}) is needed to detect advection based on the non-uniformity of heat flux determined from thermal data extending to ~100 mbsf (Fig. 11.1*b*). Conventional oceanic heat flow probes are generally ≤ 5 m long, and up-flow rates $> 10^{-8}$ m s^{-1} (0.3 m yr^{-1}) are required to cause a resolvable curvature in plots of temperature versus depth over this depth range. In addition, surface probes can only detect curvature due to up-flow; thermal gradients resulting from down-flow at equivalent rates will appear to be conductive when measured with short probes, although they will be anomalously low (Figs. 11.1*b*, *c*). A plot of thermal gradient versus depth (Fig. 11.1*d*) is often helpful in evaluating the consistency of deviations from conductive conditions.

Equation (11.1) does not explicitly include advection of heat across the confining layer boundaries. The boundary temperatures are fixed and the thermal gradients immediately adjacent to the boundaries indicate the total heat flux through the layer. For upward flow,

←

Fig. 11.1 Influence of vertical fluid flow on thermal state of a confining layer with fixed-temperature boundary conditions and various flow rates (modified from Bredehoeft and Popadopulos, 1965). (*a*) Cartoon of system configuration, with layer thickness, L, thermal conductivity, λ, upper boundary held at T_{top} and bottom boundary held at T_{bot}. (*b*) Calculated thermal structure within a 100-m-thick layer, with $T_{\text{top}} = 2\,^{\circ}\text{C}$, $T_{\text{bot}} = 22\,^{\circ}\text{C}$, and $\lambda = 1$ W m^{-1} °C, based on Eqn. (11.1). (*c*) Detail plot of upper 10 m of the layer. Upward fluid flux of 0.3 m yr^{-1} or more is generally needed to detect fluid flow within marine sediments collected in this depth range, based on the non-linearity induced by advective heat transport. Downward fluid flow may be manifested as low (but apparently conductive) heat flow. (*d*) Detail plot of upper 10 m of the confining layer showing variations in thermal gradient with depth. Relative gradient is calculated as apparent values measured at 10-cm intervals divided by the conductive gradient across the 100-m-thick layer. Upward flow increases the gradient near the upper boundary, and reduces the gradient near the lower boundary. (*e*) Total heat flux (conductive and advective) through a 100-m-thick layer with fixed-temperature boundary conditions. Total seafloor heat flux increases without limit with increasingly rapid upward seepage, and rapidly goes to zero for the case of rapid downward seepage. The two boundaries function as infinite heat sources or sinks. An alternative formulation limits total heat flow (Sleep and Wolery, 1978).

the upper boundary serves as an infinite heat sink; the faster the seepage rate, the steeper the thermal gradient at the upper boundary and the greater the total heat flux (Fig. 11.1*e*). In the same way, the lower boundary serves as an infinite heat source for the case of upward fluid flow. For the case of downward seepage, conductive heat flux at the seafloor goes to zero as the seepage rate increases (Fig. 11.1*e*).

Several workers have introduced modifications to this mathematical model. Sleep and Wolery (1978) solved the same fundamental one-dimensional heat flow equation as Bredehoeft and Papadopulos (1965), but applied a fixed heat flux boundary condition, which may be more representative in some environments. Lu and Ge (1996) modified (11.1) by relaxing the requirement that all fluid and heat flows vertically, and allowed lateral (sub-horizontal) heat transport within the confining layer to be represented through use of a heat source or sink term. As a result, temperatures within the confining layer can be greater than or less than those on both of the fixed-temperature upper and lower boundaries. This occurs if the rate at which heat is transported laterally along the layer is large relative to the rate at which heat is transported vertically. The highly layered nature of volcanic oceanic crust (Chapters 3 and 9) suggests that some ridge flank systems may host horizontal and vertical flow components of similar magnitudes, particularly if there are large lateral thermal gradients (for example, close to a spreading center or a recently emplaced seamount).

Systematic changes in thermal conductivity with depth can induce significant curvature in a conductive, steady-state, thermal gradient, and such variations must be considered before seepage rates can be inferred with confidence from thermal gradient observations. Thermal conductivity variations in shallow nature sediments on the order of $\times 2$ are common. Transient response to recent changes in bottom-water temperatures can also lead to curved thermal gradients within shallow sediments (e.g. Beck *et al*., 1985; Barker and Lawver, 2000; Von Herzen *et al*., 2001; Davis *et al*., 2003). This occurs most often within shallow water, but it can also occur in deep oceanic environments where bottom water comes from multiple sources having different temperatures. Unlike vertical fluid flow through sediments, which tends to be localized above basement highs and other features (e.g. Mottl, 1989; Giambalvo *et al*., 2000), changes in bottom-water temperatures should influence heat flow measurements made over a relatively broad area.

As described elsewhere (Chapter 16), pore-water geochemical data can also be used to estimate rates of vertical seepage. The primary differences in working with chemical data are: (i) chemical diffusivity is about three orders of magnitude less than thermal diffusivity, making chemically based flow-rate estimates commensurately more sensitive (see Fig. 6.8); and (ii) many chemical species are non-conservative, requiring that reactions be accounted for in estimating seepage rates (e.g. Mottl and Wheat, 1994; Wheat and McDuff, 1994; Giambalvo *et al*., 2002). The concentration profiles that result from non-conservative behavior may be similar to those derived by Lu and Ge (1996); steady-state concentrations may be greater than the larger of the two boundary conditions, or smaller than the lesser of the two. Because of the greater sensitivity of geochemical tracers, it is often valuable to compare estimates of seepage based on both thermal and geochemical methods. Chemical diffusivity is so low that there is little overlap in sensitivity between these methods, but if

vertical flow occurs at thermally detectible rates, fluid chemistry should be dominated by advection rather than diffusion or reaction. Conversely, pore-fluid profiles in which seepage fluxes fall within a chemically quantifiable range should coincide with thermally conductive conditions.

Several published studies have shown curved thermal gradients measured in shallow seafloor sediments. Estimates of vertical seepage fluxes from these analyses are generally 10^{-8}–10^{-6} m s^{-1} (0.3–30 m yr^{-1}). Anderson *et al.* (1979) documented curved thermal gradients within the upper 5 m of sediments from the central Indian Ocean, in an area with thin sediment cover and considerable basement relief. Thermal data were collected with outrigger probes on a large lance, and thermal conductivity measurements made on cores from the area indicated only modest changes with depth, too small to account for the non-uniform gradients. Abbott *et al*. (1981) measured permeabilities of core samples recovered from this region, and concluded that measured permeabilities were too low to allow the rates of flow suggested by thermal data with reasonable pressure gradients. Geller *et al*. (1983) documented curved thermal gradients in the upper few meters of the thick sediments of the Bengal Fan using outrigger probes. Thermal conductivity variations in this area were also insufficient to account for the observed curvature in thermal gradients, and Geller *et al*. concluded that sediment compaction and deformation may be responsible for fluid seepage through the seafloor in this region. Fisher and Becker (1991) estimated fluid seepage rates from curvature in thermal gradients in Guaymas Basin, a sedimented spreading center in the Gulf of California, using a thin, 2-m-long probe. This study did not include thermal conductivity measurements, but earlier work in the region suggested little change with depth in the upper 2–3 m. All of these studies were made where changes in bottom-water temperatures are unlikely to explain the curved thermal gradients, and all showed considerable spatial variability in apparent seepage rates. Non-uniform gradients have also been reported in the equatorial Pacific (Mayer *et al*., 1985), but with no definitive explanation other than the possibility of upward seepage of pore water.

Evidence for downward seepage has also been found. Abbott *et al*. (1984) studied core samples, pore-fluid chemistry, and heat flow from the Guatemala Basin, and found evidence for downward fluid flow into the sediments at low velocities. Similar interpretations of slow downflow have been made on the basis of chemical, thermal, and pore-pressure measurements in other ridge flank settings (McDuff, 1981; Langseth *et al*., 1984; Mottl, 1989; Langseth *et al*., 1992; Fisher *et al*., 2001).

While these results are interesting, curved thermal gradients in shallow sediments indicative of vertical fluid seepage are relatively rare. In most areas, low sediment permeability (Chapter 6) and the modest hydrothermal forces available to drive fluid flow (Chapter 8) generally do not result in thermally significant seepage through shallow sediments. For example, hundreds of heat flow measurements have been made over the sedimented northern Juan de Fuca Ridge and flank (Davis and Villinger, 1992, Davis *et al*., 1992, 1999; Stein and Fisher, 2001). This is a setting where fluid seepage might be thought likely, since pressure and thermal gradients are relatively high and some sediment (turbidite) layers are coarse grained. Instead, thermal conditions in the shallow sub-surface throughout this

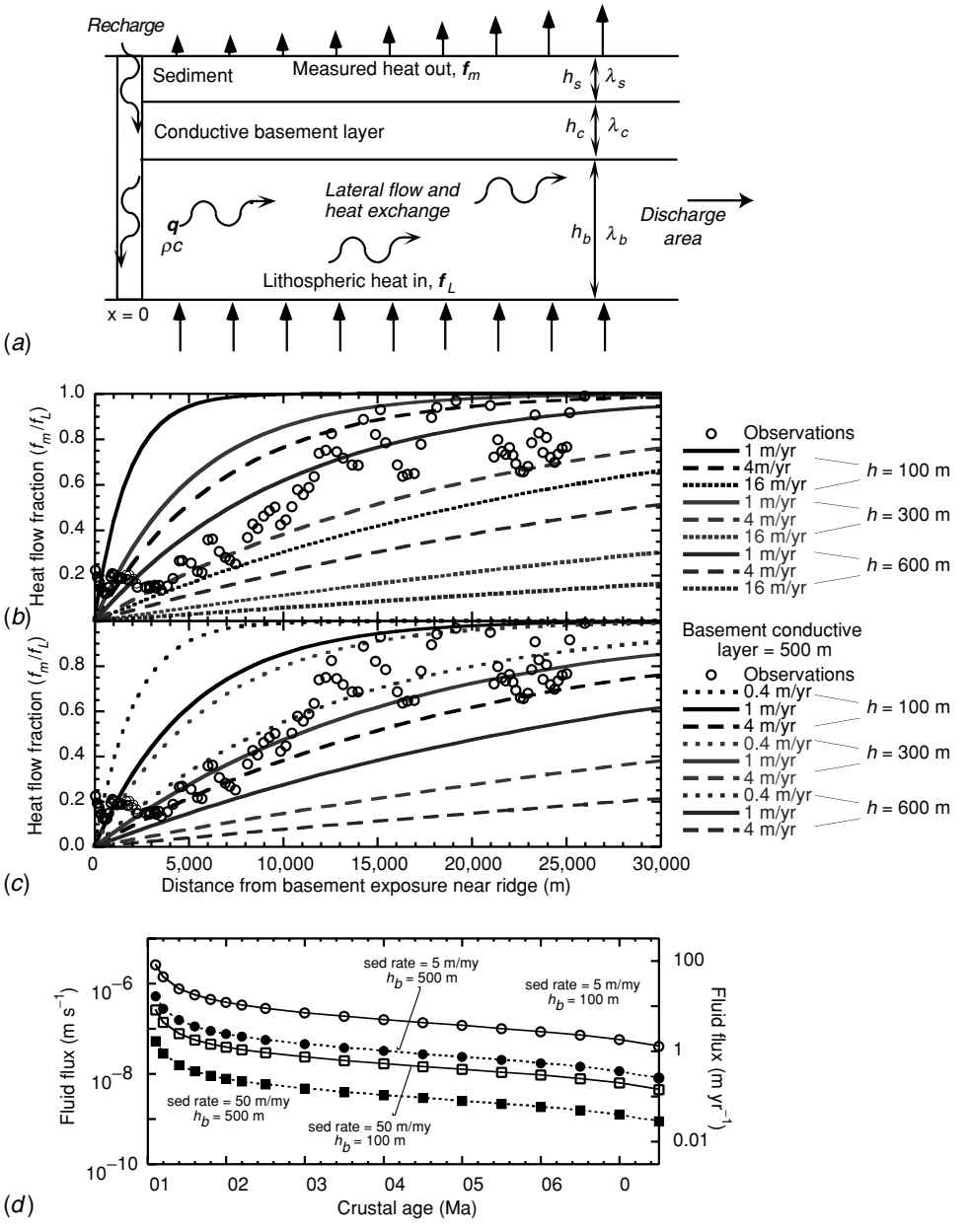

Fig. 11.2 The well-mixed aquifer model in concept and application. (*a*) Cartoon showing configuration for the well-mixed aquifer model (Langseth and Herman, 1981), including addition of a conductive layer within upper basement (Rosenberg *et al*., 2000). Fluid recharges the basement aquifer at 0 °C and flows laterally toward a discharge region, the location of which is unspecified, gaining heat from the underlying lithosphere along the way. The fluid within the aquifer is defined to be vertically isothermal;

region are conductive (except immediately adjacent to hydrothermal vent sites; e.g. Stein and Fisher, 2001). The permeability of fine-grained terrigenous sediments appears to be sufficiently low (Chapter 6) to keep seepage rates well-below thermal detectability (e.g. Davis *et al*., 1992; Wheat and Mottl, 1994).

In summary, while it is possible to detect curvature in thermal gradients associated with vertical fluid seepage and to use this information to estimate seepage rates, other possible explanations should be evaluated before fluid seepage is inferred and rates are estimated. Corrections should be made to account for thermal conductivity variations with depth. It is also important to verify that seepage rates apparent from curved thermal gradients are consistent with sediment properties and available driving forces. In several studies cited above, analysis of sediment properties suggests that unrealistically high driving forces would be required to sustain upward seepage at rates inferred from thermal data. Giambalvo *et al*. (2000) looked for evidence that upward seepage may modify sediment properties (in particular, increase permeability) through diagenesis or measurable physical processes, but could find no evidence that this occurred within fine-grained turbidites or hemipelagic sediments. This does not mean that such processes do not occur in some environments, but it does suggest that researchers should be cautious in using thermal data alone to infer fluid seepage rates. It is ideal to collect and analyze pore-fluid profiles from the same sites where curved thermal gradients are found, since thermally significant fluid flow rates should result in pore-fluid chemistry that is dominated by advection. Although there are several published examples of curved thermal gradients that could result from fluid flow, there are few data sets that combine thermal, chemical, and hydrogeologic observations so as to allow confident estimation of seepage rates.

11.2.3 Lateral rates of flow

In a study of heat flow in the Brazil Basin, western Atlantic Ocean, Langseth and Herman (1981) introduced the well-mixed aquifer (WMA) model for estimating rates of lateral fluid

←

this emulates efficient local mixing. (*b*) Comparison between seafloor heat flow observations from the eastern flank of Juan de Fuca Ridge (Davis *et al*., 1999) and calculations based on the well-mixed aquifer model (Langseth and Herman, 1981), assuming various flow rates and thicknesses for the hydrothermal layer. Heat flow values have been normalized by dividing by values predicted using a one-dimensional conductive cooling model (Parsons and Sclater, 1977), and plotted versus distance from the area of significant basement exposure to the west (assumed recharge area). (*c*) Comparison between seafloor heat flow observations and calculations based on the modified well-mixed aquifer model (Rosenberg *et al*., 2000), assuming various flow rates and thicknesses for the hydrothermal layer, and a conductive basement layer 500 m thick. The inclusion of a conductive basement layer allows slower fluid velocities to explain the general pattern of seafloor heat flow observations. (*d*) Calculated rates of mean fluid flow based on consideration of the global heat flow anomaly for seafloor of various ages, different depths of circulation, and a range of sedimentation rates (modified from Fisher and Becker, 2000).

flow. The model is based on a one-dimensional, steady-state consideration of coupled heat and fluid flow (Fig. 11.3), with water flowing laterally and capturing heat entering the system from below. Close to the point of fluid recharge, fluid temperatures will be relatively low; as the fluid moves away from the recharge area, it acquires a temperature consistent with heat input from below, the depth of circulation, and the thermal properties of the fluid–rock system.

The upper oceanic crust is idealized as a horizontally layered system, with a conductive boundary layer (sediments), underlain by an aquifer within which thermally significant transport occurs (shallow basement). Water is supplied to one end of the layer at the temperature of bottom-water, and heat is exchanged during lateral flow (Fig. 11.3*a*). The aquifer layer is assumed to be well-mixed vertically, having a temperature determined by the balance between heat entering from below and leaving through the top of the system. Temperature is thus a function only of horizontal position. The steady-state heat balance for this system is:

$$h_b\lambda_b\frac{\mathrm{d}^2T}{\mathrm{d}x^2} - h_b\boldsymbol{q}\rho c\frac{\mathrm{d}T}{\mathrm{d}x} + f_L - f_m = 0 \tag{11.2a}$$

where the first term is lateral heat conduction, the second term is lateral heat advection, the third term is heat flux in at the base of the aquifer, and the fourth term is heat flux out at the top (measured conductive heat flux at the seafloor). If bottom-water temperature is assumed to be 0 °C and sediment thermal conductivity is constant with depth, measured seafloor heat flux is defined as $f_m = K_s T/h_s$. If lateral heat conduction is small relative to the other terms (a reasonable assumption if the lateral flow rate is large and there are no local magmatic heat sources to generate large lateral thermal gradients), the first term in (11.2a) can be ignored and the solution is:

$$\frac{f_m}{f_L} = 1 - \mathrm{e}^{-Ax} \tag{11.2b}$$

where $A = K_s/(h_b h_s q\rho c)$.

The critical information required to compare predictions to observations using this model is: measured seafloor heat flux, the distance from the measurement points to the site of recharge, the thicknesses of the confining layer and the permeable rock layer through which fluid flows laterally, estimated heat input from below the aquifer, and thermal properties of the sediment and rock–fluid system. In the Brazil Basin, application of the well-mixed aquifer model yielded estimated lateral fluid flux on the order of 10^{-9}–10^{-8} m s^{-1} (0.03–0.3 m yr^{-1}) for an aquifer 1 km thick (Langseth and Herman, 1981). Assuming an effective porosity in basement of 1–10%, this range of fluxes indicates average velocities on the order of 10^{-8}–10^{-6} m s^{-1} (0.3–30 m yr^{-1}). This approach was subsequently used to estimate lateral flow rates in the eastern equatorial Pacific Ocean (Baker *et al.*, 1991), below a sediment pond on the western flank of the Mid-Atlantic Ridge (Langseth *et al.*, 1984; Langseth *et al.*, 1992), on the eastern flank of the Juan de Fuca Ridge (Davis *et al.*, 1999), and in the Alarcon Basin, Gulf of California (Fisher *et al.*, 2001).

The well-mixed aquifer model has been extended and applied in additional ways. For example, Rosenberg *et al*. (2000) relaxed the requirement that thermally significant lateral flow occur immediately below the sediment layer in uppermost basement (Fig. 11.3*a*). Because it is assumed that fluid enters the lateral flow layer at bottom-water temperature, deeper circulation allows more efficient extraction of heat from the upper lithosphere. The solution is the same as that derived by Langseth and Herman (1981), except that the parameter, A, is redefined to include the thickness and thermal conductivity of the conductive basement layer above the aquifer. In another example, Davis *et al*. (1999) included a high-conductivity proxy for the effects of lateral convective mixing as well as local variations in sediment thickness (not included in the well-mixed aquifer formulation), although this was done via a numerical model, not with the analytic solution of (11.2).

Calculations based on the well-mixed aquifer model are compared to field observations in Fig. 11.3. Seafloor heat flow data are from the eastern flank of Juan de Fuca Ridge (see Chapter 8 for additional discussion of the setting). Analytical solutions were generated based on models that exclude and include a conductive boundary within upper basement (Figs. 11.3*b* and *c*, respectively). Lateral fluxes on the order of 1–4 m yr^{-1} are required by the model if fluid flow occurs within the upper 100–600 m of basement. Values $\times 10$ lower are consistent with observations if the top of the hydrothermal layer is at a depth of 500 m into basement. This efficiency arises from the flow and heat exchange taking place with a greater temperature difference. Fisher and Becker (2000) applied the well-mixed aquifer on a global basis to estimate typical rates of circulation and available driving forces, and thus basement permeabilities, required to explain the global ridge flank thermal anomaly (see Chapter 10). These calculations were based on linking available driving forces to the thickness of the sediment section (varies as a function of basement age, using a range of sediment accumulation rates), thickness of the basement aquifer, temperature of the aquifer (varies with sediment thickness, aquifer thickness, and basement age), and distances between fluid recharge and discharge sites. Even with a large range in likely sediment and basement properties and system geometries, these calculations yielded a relatively narrow range of characteristic lateral fluid fluxes of 10^{-8}–10^{-6}m s^{-1} (0.3–30 m yr^{-1}) for seafloor younger than 20 Ma, decreasing to 10^{-9}–10^{-7}m s^{-1} (0.03–3 m yr^{-1}) for seafloor between 40 and 65 Ma (Fig. 11.2*e*).

Baker *et al*. (1991) adapted the well-mixed aquifer model for use with geochemical data in the Eastern Equatorial Pacific Ocean, reasoning that the loss of solutes from basement fluids to sediments was mathematically equivalent to conductive loss of heat. They recognized that pore-fluid compositions within thick sediment layers (400–500 m) were bounded by bottom-water compositions at both the top and the bottom of the sediment layer. Qualitatively, this required that basement pore fluids be relatively young, since these fluids had not had an opportunity to react significantly with basement. Quantitatively, Sr and $^{87}Sr/^{86}Sr$ ratios allowed estimates of basement residence times on the order of 10,000–30,000 years. Assuming typical distances between recharge and discharge sites of 20–200 km (a weakly constrained estimate of the characteristic outcrop spacing in the area), fluxes on the order of 10^{-7}m s^{-1} (3 m yr^{-1}) are suggested.

Elderfield *et al*. (1999) use a similar approach to estimate average lateral fluid flow velocities within uppermost basement along a transect of sites on the eastern flank of the Juan de Fuca Ridge. Pore fluids were collected from sediments just above basement, and assumed to be in equilibrium with underlying basement fluids. Based on (i) sulfate, chloride, and radiocarbon analyses, (ii) the spacing between sites, and (iii) a plug-flow (no dispersion) model for solute transport, lateral fluid flow velocities in upper basement are on the order of 2 m yr^{-1}, with net transport from west to east, a direction consistent with seafloor heat flow data (Davis *et al*., 1999). Assuming an effective porosity in basement of 1–10%, the lateral flux is 0.02–0.2 m yr^{-1}, significantly lower than estimated from thermal constraints.

One difficulty with applying geochemical age estimates to fluids in oceanic basement is that corrections are needed to account for solute loss to surrounding, hydrologically inactive regions by diffusion and mixing (e.g. Sanford, 1997; Goode, 1996; Alt-Epping and Smith, 2001; Bethke and Johnson, 2002; Park *et al*., 2002). Similar corrections generally are not required for flow rates estimated using heat as a tracer because of the relative efficiency of thermal conduction; this also helps to explain why dispersion is generally neglected in numerical models of coupled heat and fluid flow (Chapter 12).

There are two distinct approaches that have been used to estimate the magnitude of tracer losses in heterogeneous systems, both of which suggest that age corrections appropriate for seafloor hydrothermal systems are likely to be large, on the order of $\times 10$ to $\times 100$ or more (Sanford, 1997; Bethke and Johnson, 2002). The analysis of Bethke and Johnson (2002), based on the "age mass" concept of Goode (1996), yields the smallest age correction. Imagine that a packet of circulating water within an aquifer suffers diffusive loss of "youth" to surrounding, water-bearing but less permeable rocks during transport. The fluid velocity within an aquifer sandwiched between confining (stagnant) layers, estimated from apparent ages at two locations along a flow path, should be calculated as:

$$\boldsymbol{u} = \left[\frac{(1 + F)\,\Delta x}{\Delta t_a} \right] \tag{11.3}$$

where $F = (n_{\mathrm{con}} h_{\mathrm{con}})/(n_{\mathrm{aqf}} h_{\mathrm{aqf}})$, n = porosity, h = layer thickness, subscripts aqf and con refer to the aquifer and confining layers, respectively; Δx is the lateral spacing between sample locations; and Δt_a is the apparent age difference between fluids at each location. It is initially surprising that the magnitude of the correction does not depend on either the fluid velocity or the diffusivity of the aquifer or confining layer. This results from the assumption that, after a sufficiently long time following recharge, the loss of age mass from the primary flow channels reaches steady state. The correction necessary to account for this loss is based entirely on F, the ratio of the volume of water within the stagnant regions to the volume of water within the aquifer. Note that (11.3) reduces to the plug-flow approximation if $F = 0$. The correction required by this equation would be appropriate for both conservative and reactive tracers.

Figure 11.3 illustrates the magnitude of the correction appropriate for the eastern flank of Juan de Fuca Ridge. The system is somewhat more complex than that described by Bethke and Johnson (2002), in that lateral flow is thought to occur mainly within shallow basement, so the confining layers above the aquifer (marine sediments) and below the aquifer (less permeable basement) have different properties. If we assume reasonable values for aquifer effective porosity (1−10%), aquifer thickness (10–500 m), confining layer porosity (1−5% for underlying basement, 50–60% for overlying sediments), and confining layer thickness (1,000 m for underlying basement, 200 m for overlying sediments), the appropriate correction factor for this hydrogeologic system is 2–50 (Fig. 11.3*b*). This is likely to be a low-end estimate of the necessary correction because (i) the confining layer below the shallow basement aquifer is many kilometers thick (making the volume of water in the confining layer even larger than assumed); and (ii) these calculations neglect the influence of flow channeling within the aquifer itself (isolation of most flow within a small fraction of the most permeable regions), which would reduce effective porosity.

The theory developed by Sanford (1997) for interpretation of radiocarbon ages from aquifer fluids, rooted in concepts introduced by Sudicky and Frind (1981), is also based on the idea that most fluid flow is focused within regions that are surrounded by stagnant layers in which transport is dominantly diffusive. A stagnant zone "width factor" is defined as $w = \tanh(h_s\sqrt{\lambda/K_m}/2)$, where h_s = thickness of stagnant layers, K_m = molecular diffusion within this zone, and λ = decay constant for radiocarbon. The rate of diffusive loss is calculated as:

$$\lambda' = \left[2w\sqrt{\lambda K_m}/\left(nh_a\right)\right] \tag{11.4}$$

where n = aquifer porosity and h_a = aquifer thickness. The relative importance of diffusive to radiometric loss is expressed by the ratio λ'/λ. Typical values of λ'/λ noted for "volcanic rock layers" and "fractured rocks" are on the order of 10^2-10^5 (Sanford, 1997). Corrected fluid velocities ($\boldsymbol{u}_c$) based on radiocarbon measurements are calculated from uncorrected age values as: $\boldsymbol{u}_c = (\Delta x/\Delta t_a)(\lambda + \lambda'/\lambda)$. As the value of λ' increases, the correction factor goes to λ'/λ (Fig. 11.3*c*).

The rate of diffusive loss predicted by (11.4) depends on the thicknesses of both aquifer and stagnant layers, values that can be estimated from core and borehole observations. For example, lithologic and electrical resistivity logs from DSDP/ODP Hole 395A were compared by shipboard scientists after an initial phase of drilling and experiments and interpreted to indicate a series of vertically distinct, basaltic flows (Matthews *et al*., 1984). Each flow unit is characterized by greater electrical resistivity at the base and lower electrical resistivity at the top, interpreted to indicate an increase in porosity in rocks deposited during the final stages of each effusive event. Temperature logs collected soon after drilling (Becker *et al*., 1984) indicated that bottom water was being drawn down Hole 395A, and additional geophysical data were collected during a subsequent visit (Becker *et al*., 2001). The spontaneous potential (SP) log was used to locate intervals within Hole 395A into which borehole water flowed. Deflections in the SP log clearly correlate with the tops of individual

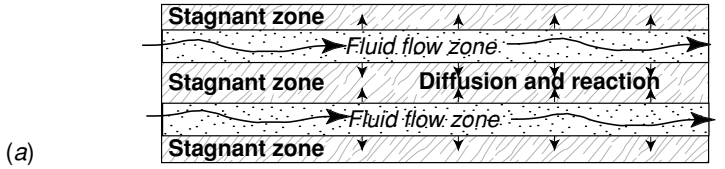

(*a*)

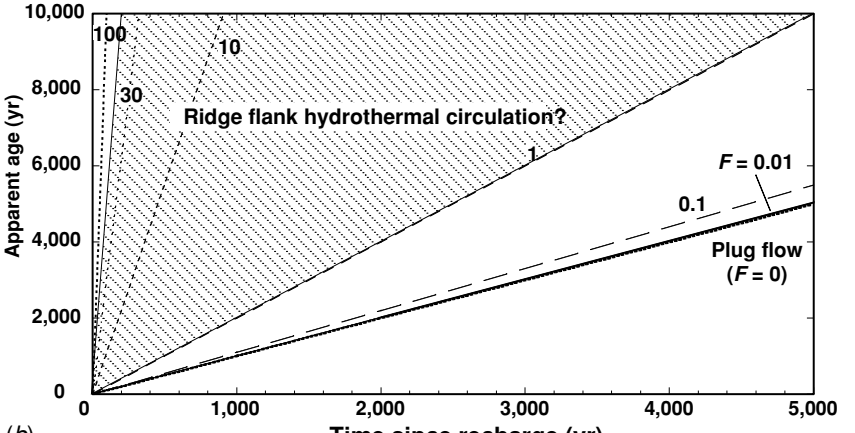

(*b*)

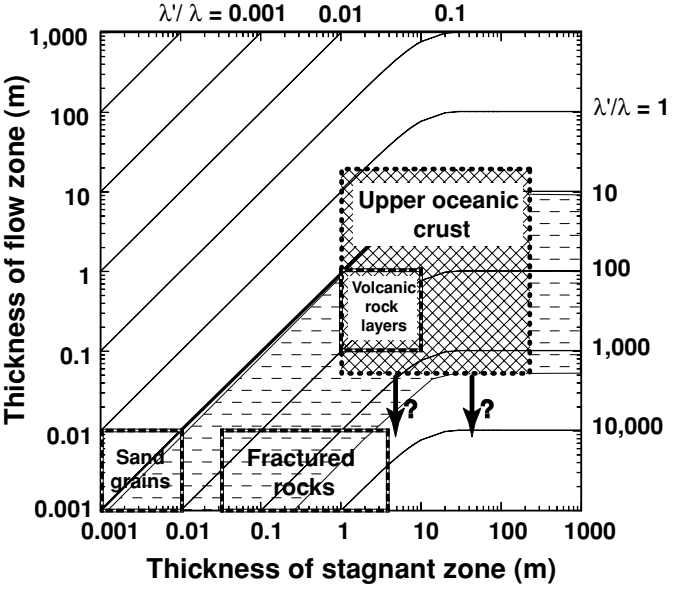

(*c*)

Fig. 11.4 (*a*) Schematic illustration showing how fluid flow through thin regions surrounded by confining (stagnant) zones can lead to loss of tracers. (*b*) Calculations of apparent age of water versus actual time since recharge, with different values of F, the ratio of the volume of water within confining layer(s) to the volume of water within the aquifer (Bethke and Johnson, 2002). The region indicated

resistivity sequences, suggesting that these thin layers, independently interpreted based on lithologic and resistivity data to have higher porosity, are also the most hydrologically active intervals. The typical thicknesses of the most and least hydrologically active sections of this borehole are on the order of 1–10 and 10–100 m, respectively (Fisher, 2003). Similar scales of layering, on the basis of combined geological, geochemical, and geophysical observations, have been noted in numerous other DSDP and ODP drill-holes (Larson *et al*., 1993; Alt, 1995; Bach *et al*., 2003).

Initial consideration of the Sanford (1997) analysis suggests that correction factors on the order of $\times 10$ to $\times 1{,}000$ should be applied to fluid velocities estimated from plug-flow interpretations of geochemical tracer experiments (Fig. 11.3*c*), but these corrections may be too low. In kilometer-scale tracer studies within the Mirror Lake fractured rock system, Becker and Shapiro (2000) and Shapiro (2001) have shown that effective chemical diffusivity of the rock matrix is at least 3×10^{-8} m^2 s^{-1}, a full order of magnitude *greater* than the diffusivity of the tracer in water. This result contrasts with the standard concept of diffusive transport within a porous medium, in which the effective diffusivity is lower than that for the solute in water, often by an order of magnitude or more (depending on the effective porosity and tortuosity of the pore network). The documented range in fracture transmissivity at the Mirror Lake field site is six orders of magnitude (Shapiro and Hsieh, 1998), and the high effective diffusivity is thought to result from preferential migration of tracer along the most permeable fractures, which are generally well connected over relatively short distances. Thus the high effective diffusivity essentially results from a component of hydrodynamic dispersion that is independent of fluid flow velocity. If the effective diffusivity of geochemical tracers in ridge flank hydrothermal circulation systems is also greater than that for free water, a distinct possibility within a heterogeneous, fractured aquifer system, then the diffusive loss correction that needs to be applied to ^{14}C data would result in λ'/λ values considerably greater than $\times 1{,}000$ (Fig. 11.3*c*).

Thus fluid velocities and fluxes estimated from plug-flow interpretation of geochemical observations on the eastern flank of Juan de Fuca Ridge are likely to be underestimates. Correction by a factor of $\times 10$ to $\times 100$ would make geochemical estimates similar to those based on thermal data, and would indicate average fluid velocities on the order of hundreds to thousands of meters per year. This is a very rapid fluid velocity in geological terms and suggests that both passive and active tracer experiments conducted at a large scale should be possible within ridge flank hydrothermal systems. This result also has important

←

by the diagonal shading is that which seems likely for several ridge flank hydrothermal systems, requiring corrections on the order of 2–50. (*c*) Illustration of corrections needed for ^{14}C data in order to estimate actual fluid ages, based on the thickness of flow zones and stagnant zones (modified from Sanford, 1997). The value $\lambda'/g\lambda$ is essentially the ratio of diffusive loss to radioactive decay, and is the magnitude of the correction that should be applied to estimates of water age based on ^{14}C analyses of basement pore fluid. Observations of crustal lithostratigraphy and *in situ* measurements of crustal properties indicate that $\lambda'/g\lambda$ is at least 10–1,000, and field estimates of dispersivity from fractured aquifers (discussed in the text) suggest that even larger corrections may be needed.

implications for the nature of water–rock interactions and the cycling of nutrients within ridge flank reservoirs, since it would imply relatively short fluid residence times.

11.2.4 Hydrothermal residence times

Researchers have attempted to estimate hydrothermal fluid residence times using both thermal and chemical tracers. Kadko and Moore (1988) and Kadko and Butterfield (1998) estimated hydrothermal residence times on the Juan de Fuca Ridge using radium. These studies suggest that fluids spend on the order of several years interacting with host rock at elevated temperatures. Other researchers have based their estimates on energy or geochemical mass-balance considerations (Davis and Fisher, 1994; Humphris and Cann, 2000). Fisher (2003) combined these results with additional estimates of hydrothermal residence times, yielding estimates in general agreement with earlier calculations.

Residence time calculations require estimates of both reservoir size and steady-state flux. Geochemical mass balance considerations led to estimates of the volume of fluid required to produce ore deposits in Middle Valley, northern Juan de Fuca Ridge (Davis and Fisher, 1994) and at the main hydrothermal field at TAG (Humphris and Cann, 2000), 5×10^8 and 4×10^8 m^3, respectively. Instantaneous heat budget estimates for these regions, the Broken Spur segment of the Mid-Atlantic Ridge, and the main field of the Endeavour Segment, Juan de Fuca Ridge, were provided by these studies and by Baker *et al*. (1996), Murton *et al*. (1999), and references therein. Heat flow was converted to equivalent mass and volume flow by assuming characteristic fluid properties (density $= 675$ kg m^{-3}, heat capacity $=$ 6400 J kg^{-1} K^{-1}, and temperature drop from reaction zone to seafloor $= 350\,^{\circ}$C).

Independent estimates of hydrothermal reservoir sizes as a function of mean spreading rate were based on considerations of the likely depth extent, width off axis, and effective porosity of the crust hosting the primary circulation system (Fisher, 2003). It was assumed that the depth extent of the reservoir scales with spreading rate ($z_{\max} = 5$ km, slow spreading; $z_{\max} = 1$ km, fast spreading), based on the observed inverse relation between spreading rate and depths to both magma lens reflectors and measurable earthquakes (e.g. Huang and Solomon, 1988; Kong *et al*., 1992; Purdy *et al*., 1992; Phipps Morgan and Chen, 1993; Chen and Phipps Morgan, 1996; Wilcock and Fisher, 2003). It was also assumed that the hydrothermal reservoir is wider at slower spreading ridges, based on the presence of a wider neovolcanic zone and more extensive axis-parallel faulting in these settings. Finally, it was assumed that effective porosities within the hydrothermal reservoir are between 1 and 10%, a reasonable range for fractured rock.

Given these ranges of parameters, estimated reservoir sizes are on the order of 2×10^7 to 2×10^8 m^3 km^{-1} of ridge for a fast-spreading ridge (full spreading rate $= 160$ mm a^{-1}), and 5×10^8 to 5×10^9 m^3 km^{-1} of ridge for a slow-spreading ridge (full spreading rate 20 mm a^{-1}), values that straddle the geochemical estimates described earlier for Middle Valley and TAG. Additional estimates of steady-state heat flow (and thus mass and volume flow) come from consideration of the global distribution of known vent sites (e.g. Baker, 1996; Baker *et al*., 1996). These estimated reservoir volumes and hydrothermal budgets

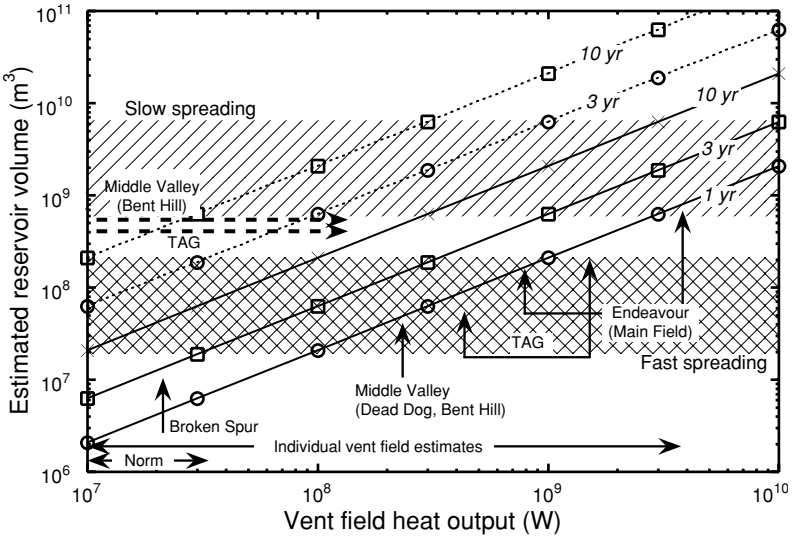

Fig. 11.4 Calculations and estimates of ridge crest hydrothermal reservoir volumes and heat output, and resulting fluid residence times in the sub-surface (Fisher, 2003). Estimated reservoir volumes are shown per kilometer of ridge crest, based on seafloor spreading full rates of 20–160 mm yr^{-1} ("slow spreading" and "fast spreading," respectively). Estimates of reservoir volumes needed to produce massive sulfide deposits are labeled with horizontal arrows for TAG and Middle Valley–Bent Hill. Vent field heat flow estimates are from Baker *et al*. (1996), Murton *et al*. (1999), Humphris and Cann (2000), and references therein, for Broken Spur, Middle Valley–Dead Dog and Bent Hill, TAG, and the Endeavour Segment – Main Field. The heat output range labeled "Norm" indicates normalized high-temperature vent field output (corrected for the fraction of ridge hosting high-temperature circulation at any time (Baker and Urabe, 1996). Diagonal lines are steady-state fluid residence times based on these values and effective porosities of >1% (solid lines) or 10% (dashed lines). Ten-year residence time with effective porosity of 1% is equivalent to one-year residence time with effective porosity of 10%, since the same amount of water–rock interaction is assumed. These calculations show that residence times on the order of years (as opposed to weeks or decades) are consistent with a wide range of geochemical and geophysical considerations.

are consistent with hydrothermal residence time, t_r = 1–10 years (Fig. 11.4). There is considerable uncertainty in many of the parameters used to estimate these residence times, but ongoing field programs focusing on fluxes, hydrogeological properties, and flow scales will help to refine these calculations.

These high-temperature hydrothermal residence times are considerably shorter than estimates derived for ridge flank hydrothermal systems, on the order of 10^4 years (Baker *et al*., 1991; Elderfield *et al*., 1999). However, as noted previously, residence time estimates for ridge flanks based on geochemical estimates and a plug-flow approximation almost certainly require correction by at least a factor of ×10, and perhaps by a factor of ×100 to ×1,000 or more. Interestingly, such corrections would result in hydrothermal residence time estimates for ridge flank hydrothermal fluids that are about the same as

those from spreading centers, although there is no particular reason why this might be expected.

11.3 Patterns of fluid circulation

11.3.1 Heat flow observations and the occurrence of "cellular convection"

Elder (1965) was among the first to speculate that widespread hydrothermal circulation could advect significant quantities of heat from young oceanic lithosphere. Although there were few direct observations allowing quantification of this process at the time, inferences were drawn from related studies of buoyancy-driven convection. Lapwood (1948), Wooding (1960), and Nield (1968) evaluated conditions necessary for the onset of convection, including the imposition of various pressure and temperature boundary conditions. These and other studies also assessed the shape of convection cells within homogeneous, porous systems heated from below.

Lister (1972) analyzed heat flow measurements from near the Juan de Fuca Ridge, attributed the variations in observed values to hydrothermal circulation, and drew several sketches illustrating hypothetical flow paths (see Chapter 2). The convection cells in these drawings generally had an aspect ratio (cell width/cell height) near one, and showed the convection cells as two-dimensional in a ridge-perpendicular plane, parallel to the direction of spreading. Limited observational data available at the time were consistent with these ideas.

The first study that combined detailed seafloor heat flow observations with bench-top models of buoyancy driven convection, and drew explicit inferences regarding the geometry of circulation, was that of Williams *et al*. (1974). This paper and companion studies of young seafloor north and south of the Galapagos Spreading Center (Detrick *et al*., 1974; Klitgord and Mudie, 1974; Sclater *et al*., 1974), documented fundamental characteristics of young oceanic crust formed at a moderate-rate spreading center: a median valley having topographic relief of several hundred meters, abyssal hills and associated faults (generally inward dipping) that form sub-parallel to the ridge with spacing of several kilometers, and patchy sediment cover that thickens and becomes more continuous with distance from the ridge. Williams *et al*. (1974) also noted a critical pattern in seafloor heat flow: values measured along transects oriented perpendicular to the ridge (parallel to the direction of spreading) were generally suppressed below that expected based on models of conductive lithospheric cooling (e.g. Sclater and Francheteau, 1970), but showed systematic variations, with alternating regions of relatively high and low values. The amplitude of these variations was one order of magnitude, and the wavelength of variations was 5–10 km, about the same as the abyssal hill spacing.

The regularity of heat flow highs and lows led Williams *et al*. (1974) to consider the occurrence within oceanic crust of "cellular convection" organized in two-dimensional rolls having an aspect ratio close to one (Fig. 11.5). Seafloor heat flow observations could be explained by cellular convection having rising limbs below heat flow highs (sometimes

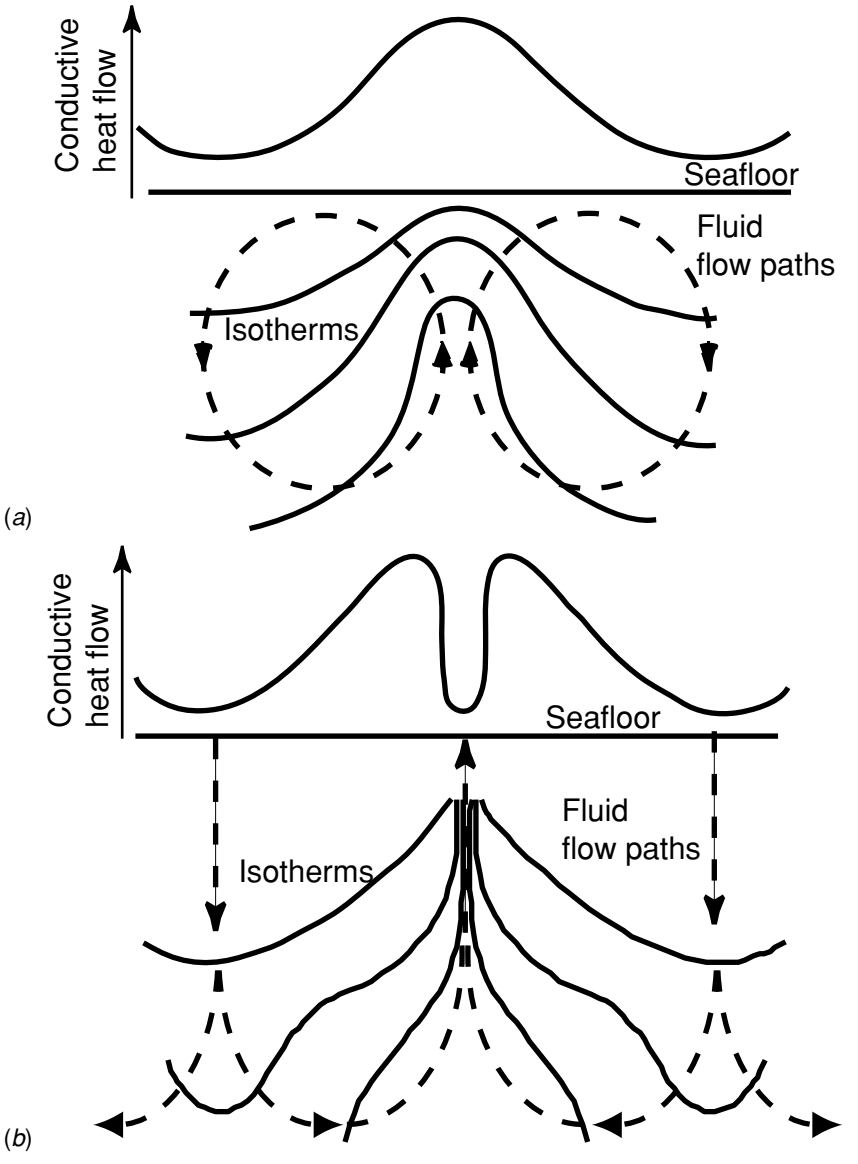

Fig. 11.5 Cartoon of hypothesized fluid convection cells and resulting seafloor heat flow (modified from Williams *et al*., 1974). Note low aspect ratio of convection cells, with depth of circulation being approximately equal to the width of the cells. (*a*) Fluid flow pathways, isotherms, and seafloor heat flow resulting from convection within basement rocks covered with a low-permeability sediment layer. (*b*) Fluid flow pathways, isotherms, and seafloor heat flow resulting from convection within basement rocks, where water can readily pass through incomplete sediment cover. Heat flow is suppressed immediately above the hydrothermal up-flow zone because conditions close to the seafloor are essentially isothermal.

associated with basement and seafloor highs), and downgoing limbs below seafloor heat flow lows (sometimes associated with basement and seafloor lows), as discussed by Lister (1972). Williams *et al*. (1974) suggested that convection "cells are approximately equidimensional." Thus it was concluded, "[w]ith our observed modulation [of seafloor heat flow values] of wavelength of 6 km, equidimensional Rayleigh cells would penetrate approximately 3 km and greater depths are certainly possible." Subsequent field studies by Green *et al*. (1981), Langseth *et al*. (1988), and others documented swaths of high and low heat flow on ridge flanks that were elongated sub-parallel to the spreading center. These observations were consistent with the idea that the primary direction of fluid circulation was perpendicular to the ridge, and that these systems could be modeled using cross-section simulations.

The first numerical studies of two-dimensional, porous media convection within mainly isotropic crustal systems were thus oriented perpendicular to the ridge (Ribando *et al*., 1976; Fehn and Cathles, 1979; Fehn *et al*., 1983). Permeability in these studies was generally made homogeneous or smoothly varying (for example, decreasing exponentially) with depth. Results of this work reinforced earlier interpretations of ridge flank (and, to some degree, ridge crest) hydrothermal systems: (i) convection cells tend to have aspect ratios near one and thus a wavelength of circulation similar to the depth of circulation; and (ii) conductive heat flow at the seafloor tends to be elevated above rising convection limbs and suppressed above downgoing limbs, allowing both the wavelength and depth extent of circulation to be inferred from measurements of seafloor heat flow. However, there are good reasons to reconsider both of these concepts, as discussed in the following section.

11.3.2 Challenges to the cellular convection concept

There are several reasons why we should not expect hydrothermal convection in the ocean floor to form cells similar to those that form in an isotropic, homogeneous porous medium: (i) the oceanic crust is strongly layered, (ii) the crustal aquifer is heterogeneous and anisotropic, and (iii) convection geometry is likely to vary over time. Oceanic crust is constructed in irregular layers (e.g. Houtz and Ewing, 1976; Purdy and Detrick, 1986; Karson, 1998, 2002; Jacobson, 1992; Smith and Cann, 1999). The uppermost few hundred meters are composed mainly of pillows, flows, and breccia, with proportions of extrusive components varying with spreading rate, proximity to fracture zones and the ends of ridge segments, and the overall robustness of magmatic processes. Deeper sections comprise mainly dikes and other intrusive rocks. Diking is most common within and near the neovolcanic zone (e.g. Smith and Cann, 1993; Delaney *et al*., 1998), but continues to some distance off-axis. The crust is modified tectonically, beginning close to the ridge and extending well off-axis (e.g. Macdonald *et al*., 1996; Blackman *et al*., 1998), providing a ridge-parallel fabric of faults and fractures that is superimposed on the sub-horizontal, layered structure established during initial construction (see Chapters 3 and 9 and references therein).

We should expect that the combination of horizontal layering and sub-horizontal to sub-vertical faulting and fracturing imposes considerable heterogeneity and anisotropy

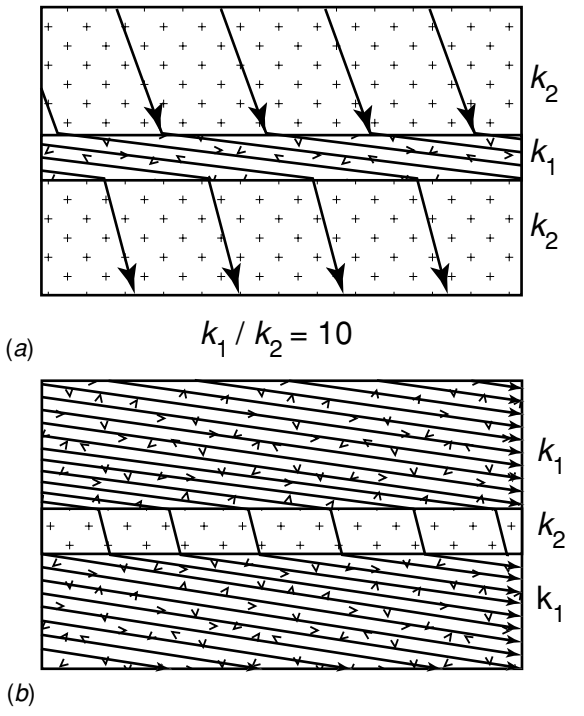

Fig. 11.6 Illustration of the importance of formation anisotropy on the dominant direction of fluid flow (modified from Hubbert, 1940). In both drawings, there is a permeability ratio of $k_1/k_2 = 10$, and the gradient driving flow is directed from the upper left to the lower right. (*a*) A thin region of high permeability between layers of lower permeability. Flow lines are refracted to flow along the high-permeability layer, remaining within this layer for as long as possible. (*b*) A thin region of low permeability between layers having higher permeability. Flow lines are refracted so as to cross the region of low permeability as rapidly as possible. In both of these cases, there would be no refraction of flow only if the gradient were oriented perpendicular or parallel to the layering.

to crustal hydrogeologic properties. Permeability anisotropy within layered sedimentary aquifers commonly exceeds $\times$10–50 (horizontal to vertical, e.g. Bair and Lahm, 1996); anisotropy within brecciated and fractured oceanic basement, associated with either sub-horizontal layering or sub-vertical faulting, may be $\times$100 or more. Anisotropy (even in the absence of heterogeneity) leads to refraction of flow lines such that the dominant fluid flow direction can be highly oblique to the gradient in driving forces (Fig. 11.6). Individual layers, fractures, and faults within natural hydrogeological systems can act as conduits for flow, barriers to flow, or both at the same time (e.g. Caine *et al*., 1996), and it is generally not possible to predict how an individual structure will influence fluid flow patterns or intensity without direct testing. Hydrothermal circulation and associated reactions impose additional heterogeneity through differential rock alteration (e.g. Alt, 1995), leading to the development of hydrogeologically distinct regions within the crust. One example of this hydrothermal "compartmentalization" in oceanic basement comes from ODP Hole

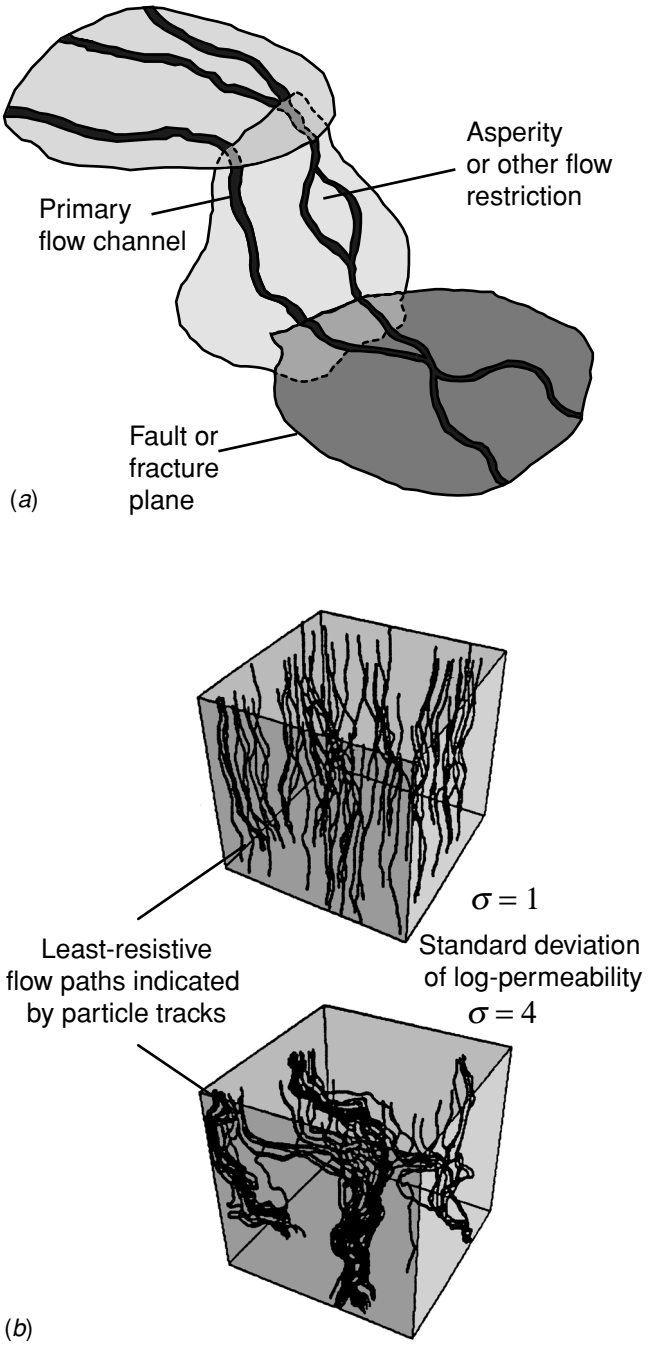

Fig. 11.7 Illustration of two processes that can lead to flow channeling (modified from Wilcock and Fisher, 2002). (*a*) At the scale of individual, intersecting fracture planes, most flow occurs along a small fraction of each fracture surface, away from asperities or other blockages (Tsang *et al*., 1991).

801C in the western Pacific Ocean, drilled into one of the oldest remaining sections of the seafloor. This crust is layered in terms of both primary lithology and secondary modification, including adjacent, alternating zones of oxidized and reduced hydrothermal alteration, glassy pillows, and massive Fe–Si precipitates (e.g. Larson *et al*., 1993; Alt and Teagle, 2003).

Heterogeneous rock systems, particularly those within fractured rock, are widely recognized to experience flow channeling (e.g. Tsang and Neretnieks, 1998), a process by which the vast majority of the fluid flow (and associated solute and heat transport) is concentrated to occur within a small fraction of the total rock volume. This process occurs on many scales (Fig. 11.7). Within individual fault and fracture surfaces, asperities block fluid flow along most of the surface (e.g. Tsang *et al*., 1991). Similarly within heterogeneous systems at a larger scale, fluid circulation tends to follow the paths that offer the least resistance for a given driving force magnitude and direction (e.g. Tsang and Tsang, 1989; Clemo and Smith, 1997). Thus the dominant flow paths are not fixed in a physical sense, but will vary as a function of the interplay between heterogeneity and driving forces. In stochastic numerical studies of three-dimensional fluid flow at a larger scale (Moreno and Tsang, 1994), it was shown that systems having a large standard deviation in permeability will develop preferential flow paths that utilize a small volume of the formation porosity. It is these variations in permeability, rather than the average value, that determine the extent of flow channeling. Because oceanic basement rocks are highly heterogeneous, particularly within the upper few hundred meters, fluid flow must be highly channeled. This interpretation is consistent with the common association between seafloor structure and hydrothermal venting (e.g. Karson and Rona, 1990; Delaney *et al*., 1992; Wright *et al*., 1995; Kleinrock and Humphris, 1996) and with the rock record of heterogeneous alteration (Chapter 15).

Hydrothermal circulation patterns within many crustal systems are also likely to vary in shape with time (to be oscillatory or otherwise unstable), given sufficiently high driving forces and permeability (Kimura *et al*., 1986; Davis *et al*., 1997), preventing delineation of characteristic shapes of convection cells. This complexity is exacerbated near the critical point for water, as within many ridge crest hydrothermal systems (Goldfarb and Delaney, 1988; Von Damm, 1995), where phase separation and the formation of vapor and/or brine can result in fluid segregation and divergence of flow paths and fluid properties, but instability is also expected under conditions documented within many ridge flank circulation systems.

Studies of the eastern flank of the Juan de Fuca Ridge identified one area that was thought to have a flat-topped basaltic aquifer buried below several hundred meters of

←

(*b*) At a larger scale, within heterogenous rock systems having the same mean permeability, flow is much more highly focused when there is a high standard deviation in log-permeability (Moreno and Tsang, 1994). This process does not depend on the absolute magnitude of mean (or effective system) permeability; even extremely permeable systems experience flow channeling, because fluids prefer to travel along the paths of least resistance.

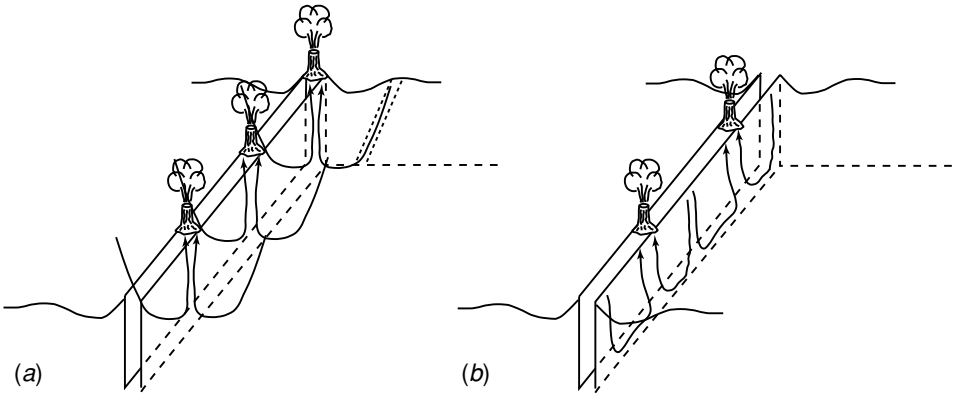

Fig. 11.8 Cartoons showing two end-member circulation geometries for both ridge crest and ridge flank hydrothermal circulation (inspired by Haymon *et al*., 1991; Delaney *et al*., 1992; Sohn *et al*., 1997). Central slot indicates either spreading axis (for ridge crest systems) or a high-angle fault (for ridge flank systems). Drawings are not to scale. Actual flow geometries are likely to be more complicated than either end member. (*a*) Across-strike flow. (*b*) Along-strike flow. Note that there are sites of fluid recharge located between up-flow zones for this circulation geometry.

low-permeability sediments. This seemed to be an ideal place to test the for the occurrence of near-unity-aspect-ratio convection cells within hydrologically isolated basement, as hypothesized to occur by Lister (1972) and Williams *et al*. (1974). Field and numerical analyses were interpreted initially to indicate that near-unity-aspect-ratio convection cells having a width and height of about 600 m were responsible for small-scale variations in seafloor heat flow (Davis *et al*., 1992, 1996; Snelgrove and Forster, 1996). However, subsequent numerical and seismic studies (Fisher and Becker, 1995; Davis and Chapman, 1996) showed that subtle variations in relief at the aquifer top could control the geometry of underlying convection and lead to the observed heat flow pattern. In a similar way, the locations of isolated basement outcrops, which provide fluid entry and exit points for many ridge flank systems, are likely to influence convection geometry (e.g. Lister, 1972; Fisher *et al*., 2002; Villinger *et al*., 2002). Although the concept of cellular convection remains rooted in many descriptive models of hydrothermal circulation, it has yet to be shown that near-unity-aspect-ratio cells are actually favored within natural seafloor systems.

11.3.3 Along-strike versus across-strike fluid flow

There is a tendency when drawing cartoons of seafloor hydrothermal circulation to collapse the crust and the associated fluid pathways into a two-dimensional cross-section oriented perpendicular to the ridge (Fig. 11.8*a*). This results, in part, from the way in which researchers developed and tested ideas about crustal formation and evolution. Early views of seafloor structure were based largely on seismic studies (e.g. Raitt, 1963) and comparison with ophiolites (e.g. Moores and Vine, 1971; Cann, 1974). Conventional reflection and refraction studies are inherently two dimensional, and commonly profiles are oriented so

as to cross perpendicular to primary structures (cross-strike) because lines sub-parallel to structure (along-strike) are usually more difficult to interpret. Also, many early studies of ophiolites focused on relations between crustal structure and spreading processes (nature of magma chamber, orientation and mode of emplacement of dikes, etc.), emphasizing cross-strike relations.

Observations of fluid circulation at spreading centers illustrate the importance of along-strike flow (Fig. 11.8*b*). Haymon *et al*. (1991) noted the alignment and consistent spacing between sites of high-temperature hydrothermal venting on the East Pacific Rise (EPR) at 9−10° N, and suggested that this could result from along-axis convection. Seafloor observations along the EPR show that axial fissures are strongly aligned sub-parallel to the ridge axis (e.g. Wright *et al*., 1995), likely imparting a hydrogeologic fabric to the upper crust. Seismic refraction studies have also indicated anisotropic (along-strike) crack distributions extending to depths of several kilometers (Dunn and Toomey, 2001). Collectively, these observations suggest that the dominant orientation of hydrothermal circulation cells on the EPR may be along axis (Haymon, 1996).

Delaney *et al*. (1992) similarly observed the association of hydrothermal vent sites on the Endeavour Segment of the Juan de Fuca Ridge with along-strike structures, an observation that has proven robust as new vent sites have been discovered (Kelley *et al*., 2001). Wilcock and McNabb (1996) noted that Endeavour Segment vent fields are elongated sub-parallel to the spreading axis, and suggested that permeability anisotropy could favor along-axis circulation cells. Hydrothermal vent fluids on the Endeavour Segment of the Juan de Fuca Ridge have chemistries indicative of substantial interaction with sediments at elevated temperatures, even though this part of the ridge is sediment free at the seafloor (Lilley *et al*., 1993; Butterfield *et al*., 1994, 1997). One explanation is that fluids interact with sediments interbedded with lavas at depth, but another option is that along-ridge transport brings hydrothermal fluids tens of kilometers along strike from the north, where the ridge is sedimented (Wilcock and Fisher, 2003). As at the EPR, seismic studies along the Juan de Fuca Ridge also detect large-scale seismic anisotropy within the upper crust (e.g. Sohn *et al*., 1997), with greater velocities in the along-axis direction, consistent with a crustal fabric established during or soon after crustal formation. Of course, actual flow geometries in these systems are likely to be complex, even three-dimensional (e.g. Travis *et al*., 1991), so delineation of individual vector components (along-strike or across-strike) may not indicate the dominant direction of fluid flow within any particular system.

There are considerably fewer studies of ridge flank hydrothermal systems that provide an indication of the importance of along-strike versus across-strike flow. As described earlier, the occurrence of elongate heat flow anomalies sub-parallel to the spreading center has been interpreted to indicate a predominantly across-strike fluid circulation direction. However, once vigorous circulation largely homogenizes temperatures in upper basement, the pattern of seafloor heat flow will mimic the distribution of basement relief and sediment thickness no matter what the dominant flow direction (Chapter 8). Although geochemical and geothermal data on the western end of the ODP Leg 168 transect (Davis *et al*., 1999; Elderfield *et al*., 1999) are consistent with a dominant flow direction from west to east

(across-strike), basement outcrops to the north and south of this transect could play an important role in guiding fluid to and from the basement aquifer. Along the eastern end of this transect, fluid exiting the top of the Baby Bare basement outcrop appears to be focused along one or more ridge-parallel faults (Mottl *et al*., 1998; Becker *et al*., 2000). In addition, pore-fluid data from uppermost basement around Baby Bare suggest an evolution in an along-strike direction, from south-southwest to north-northeast (Wheat *et al*., 2000). Heat flow data from a large basement outcrop 52 km south-southwest of Baby Bare, along structural strike, suggest that this feature may allow recharge of seawater into this part of the ridge flank hydrothermal system (Fisher *et al*., 2002). Seismic anisotropy studies on ridge flanks (Stephen, 1981, 1985) are also consistent with preferential orientation of fractures in an along-strike direction.

Several recent studies have also indicated hydrogeologic connections between ridge crests and ridge flanks. For example, Johnson *et al*. (2000) documented changes in ridge crest venting temperatures (and possibly flow rates) associated with off-axis seismicity. Davis *et al*. (2001) showed that borehole pressures on ridge flanks can respond to largely aseismic spreading at the axis. These studies suggest that there are important connections between stress state, seismic activity, and crustal properties over distances of kilometers or more, but they do not require significant fluid flow or heat flow between ridge crest and ridge flank areas. In each of these cases, strain in the plate is probably responsible for the long-distance transport of energy, with the initial hydrogeologic response being a local phenomenon (Chapter 8). The extent of heat, fluid, and solute exchange between ridge crest and ridge flank hydrothermal systems remains largely unconstrained. Quantifying these fluxes is important for understanding numerous processes, including mechanisms of heat extraction and crustal construction, and the nature of thermal rebound following the cessation of high-temperature circulation at the ridge (e.g. Chen and Phipps Morgan, 1996; Fisher, 2002)

11.3.4 Directions of fluid flow

It would seem to be a simple matter to determine the direction of fluid flow between field sites by measuring pressures in pairs of sealed boreholes, but this has been challenging because pressure differences are small (Davis and Becker, 2002). A more fundamental difficulty is that coupled heat and fluid flow problems in which fluid properties vary with pressure and temperature often cannot be solved based on a static consideration of differences in absolute pressure. Pressure is a form of potential energy, but the direction of fluid flow will follow the gradient in pressure only if: (i) permeability is either homogeneous or is anisotropic with the primary permeability aligned with the steepest gradient; and (ii) variations in fluid density occur only in the vertical direction, and surfaces of equal density correspond to surfaces of equal pressure (e.g. Hubbert, 1956; Hickey, 1989; Oberlander, 1989). Particularly in cases where pressure differences are small and there are lateral changes in fluid properties, a fully coupled solution is required to determine the fluid flow direction (e.g. Ingebritsen and Sanford, 1998).

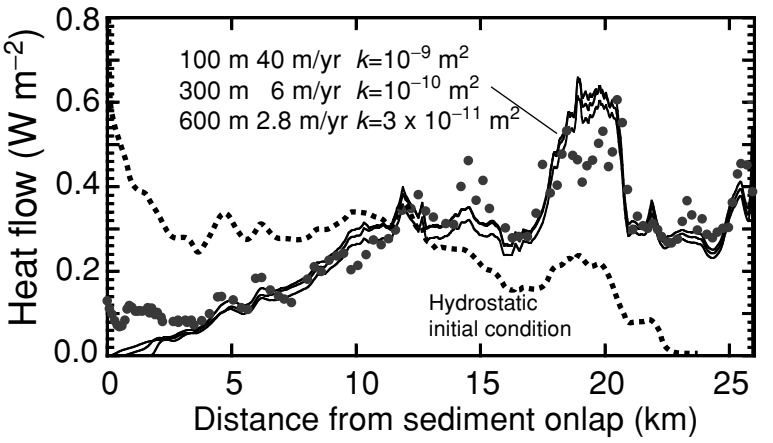

Fig. 11.9 Comparison between heat flow observations and results of transient numerical models of heat and fluid flow along the western end of the ODP Leg 168 transect (Fig. 8.3*b*). Dots show oceanic heat flow values measured with a seafloor probe (Davis *et al*., 1999). Lines indicate output from numerical models (Stein and Fisher, 2003). Models were cast using a two-dimensional domain oriented perpendicular to the ridge to the west, with sediment thickness and seafloor and basement relief based on seismic data. Fluid entered and exited the seafloor through the side boundaries. The thickness of the permeable aquifer in uppermost basement was varied from 100 to 600 m, and permeability was adjusted to allow sufficiently rapid lateral flow so as to match the general pattern of seafloor heat flow. Heat input at the base of the domain is greatest on the left, where the seafloor is youngest, and decreases to the east, with greater distance from the ridge. Dotted line shows heat flow resulting from a simulation in which the initial pressure condition was "warm" hydrostatic, based on a conductive solution. All simulations started with this initial condition resulted in flow from east to west, a direction opposite to that indicated by seafloor heat flow measurements. However, when fluid flow was initially forced from west to east, and then the forcing was discontinued, fluid continued to flow in this direction because a "hydrothermal siphon" had been established. Basement permeability was then adjusted to allow a good match between model results and observations, with the fluid flux and permeability values shown for various thicknesses of the basement aquifer.

Numerical studies of ridge flank circulation may also yield non-unique results, with predicted flow directions that depend on grid geometry and boundary and initial conditions. Fisher *et al*. (1994, 1990) showed numerical simulations of ridge flank hydrothermal circulation enhanced by basement and seafloor relief. In these studies, fluid rose from depth below the peak of basement and topographic highs and then flowed laterally down the sloping flanks of local ridges, consistent with bench-top models (Hartline and Lister, 1981). These numerical studies used a transient, integrated finite-difference model of coupled heat and fluid flow, but the first analysis was completed with a rectangular grid, similar in form to earlier studies (e.g. Fehn and Cathles, 1979), while the second analysis employed a curvilinear (non-rectangular) grid that allowed more efficient fluid and advective heat flow. A later analysis that included finer grid spacing on the flank of a buried basement ridge demonstrated that, if the basement aquifer is sufficiently permeable and is isotropic, wide convection cells will break up into smaller cells (Fisher and Becker, 1995). At one level the

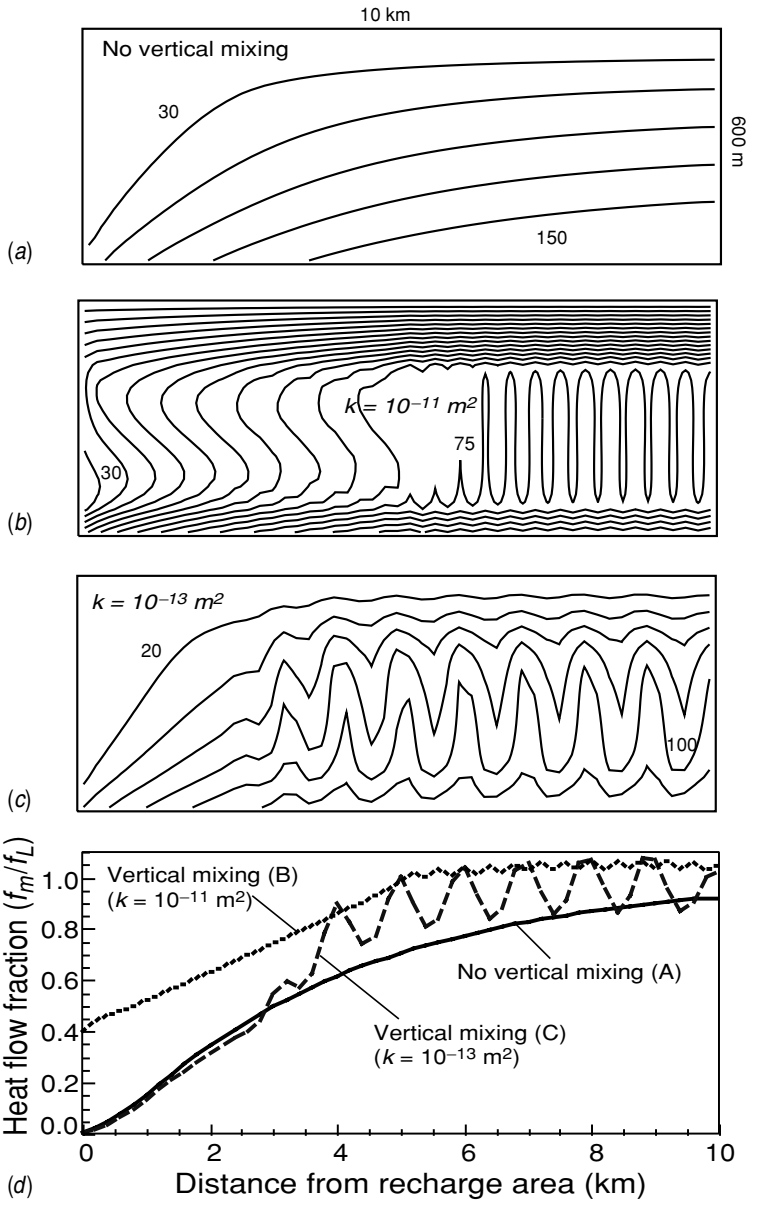

Fig. 11.10 Numerical results of coupled heat and fluid flow in an idealized, two-dimensional system, illustrating the influence of mixed convection on heat transport efficiency (Rosenberg *et al.*, 2000). All models have the same geometry, and fluid is forced to flow from left to right ($\boldsymbol{q}$ = 10^{-8}m s^{-1}, 0.3 m yr^{-1}) along a 400-m-thick basement aquifer placed below low-permeability sediments. (*a*) Temperature field for numerical solution of large-scale lateral flow with vertical mixing prevented through use of permeability anisotropy in basement. Temperature contour interval is 30 °C. (*b*) Temperature field for same case but with vertical mixing allowed; isotropic permeability in lateral-flow layer is 10^{-11} m^2, and temperature contour interval is 5 °C. Because the system is allowed

use of wider cells could be interpreted to introduce a numerical "mesh effect," but if the actual system is highly anisotropic, then the use of wide cells (which favors sub-horizontal flow) may actually be geologically realistic. This possibility requires field observatories that can distinguish between wide and narrow cell geometries, or allows an independent assessment of permeability anisotropy.

Steady-state modeling by Davis *et al*. (1997) and Wang *et al*. (1997) quantified the influence of topography and basement relief on convection in the upper oceanic basement of a ridge flank, and determined relations between crustal properties, convection geometry, and thermal and pressure homogenization within a basement aquifer. In one set of simulations, it was shown that the direction of flow relative to the hydrologic structure depends on the starting state of the numerical model. In addition, once convection becomes sufficiently vigorous so as to homogenize basement temperatures (generally a result of permeabilities so great as to also make lateral pressure gradients very small), flow in either direction can result in similar pressure and thermal conditions within shallow basement. Spinelli and Fisher (in press) simulated coupled heat and fluid transport between a buried basement ridge and trough on the eastern flank of the Juan de Fuca Ridge, and compared modeling results to date from long-term, sub-seafloor observatories (Chapter 8). New models show that the preferred flow direction at dynamic "steady state" (convection is unstable and oscillatory) depends on geological and model initial conditions when basement permeability is homogeneous. However, when most of the permeability in upper basement was concentrated within thin layers, the flow directions was always upward in basement below the buried basement high. These solutions also gave a better match to sub-seafloor observations than did models having downward flow within the buried basement ridge.

Stein and Fisher (2003) obtained a related result when they modeled a 26-km-wide section of the eastern flank of the Juan de Fuca Ridge (Fig. 11.9). Fluid could be forced to enter basement close to the ridge crest to the west and then to flow to the east, but when transient models were started with a hydrostatic initial condition (either cold or warm, based on a conductive thermal solution), the final fluid flow direction was from east to west, opposite to that inferred from heat flow and geochemical observations (Davis *et al*., 1999; Elderfield *et al*., 1999). This occurred because heat flow into the base of the grid was greatest at the western end of the domain, where the lithosphere was youngest, leading to up-flow in this area. However, once rapid flow was initiated from west to east in the transient models, through use of temporary, forced-flow boundary conditions, a "hydrothermal siphon" was established, and the small difference in basement pressure below cool and warm columns

←

to convect freely it is thermally more homogeneous than in the case with no vertical mixing. (*c*) Temperature field for same case, but with isotropic permeability in lateral-flow layer of 10^{-13} m^2. Temperature contour interval is 20 °C. Convection still occurs, but mixing is less vigorous than in the case with higher permeability. (*d*) heat flow fraction (f_m/f_L) as a function of distance from the recharge area for all three cases. The case with no vertical mixing is most efficient in suppressing seafloor heat flow, and the case with the most vigorous vertical mixing is the least efficient in suppressing seafloor heat flow.

of water (recharge and discharge sites, respectively) continued to move fluid from west to east even after forcing was discontinued.

These studies illustrate a fundamental limitation in using numerical models to infer fluid flow directions: the results of both steady-state and transient models often depend on the starting condition. In the case of transient simulations, this starting state should not be a numerical convenience; it should represent realistic geological conditions. Representing such conditions within a system that evolves over geological times poses unique challenges; taken to an extreme, the correct initial condition is established when magma upwells below the spreading center and intrusive and extrusive layers are formed.

Another complexity in characterizing the patterns and rates of fluid flow in ridge flank hydrothermal systems is the occurrence of mixed convection, i.e. local convection superimposed on rapid net throughput of fluid. Numerical analyses have shown that mixed convection occurs within a lateral-flow system when permeability is sufficiently large and isotropic (Fig. 11.10). Convective mixing helps to homogenize basement temperatures locally, but reduces the efficiency with which heat is extracted by crustal-scale lateral flow (Davis *et al*., 1999; Rosenberg *et al*., 2000; Stein and Fisher, 2003). Numerical models can be made to allow or exclude mixed convection, depending on the absolute magnitude of permeability, the degree of permeability anisotropy, aquifer geometry, and the magnitude of lateral driving forces, but it is not clear how one would test for the occurrence of this process within natural systems.

11.4 Summary and recommendations

Enormous progress has been made in the last several decades in quantifying the rates and directions of fluid flow within seafloor hydrothermal systems. Continued characterization is essential for determining the dynamics and impacts of fluid, heat, solute, and biological fluxes. There are several thermal and geochemical techniques that allow estimation of vertical fluid fluxes through sediments, and lateral fluid fluxes through basement aquifers. We should take advantage of apparent discrepancies between flow rates estimated using different methods, as these differences may help us to find flaws in analytical techniques or assumptions, or may tell us something fundamental about the nature of flow systems. Although assumptions about the isotropic, homogeneous nature of sub-seafloor hydrothermal systems allow us to apply simple models, we should continue to explore the anisotropy and heterogeneity that is to be expected in complex, geological environments. Many of these complexities result from the way in which oceanic lithosphere is created and evolves, so we should make all possible use of geological and other information that can help to guide development of increasingly sophisticated models.

We must continue to develop and apply tools that allow us to map thermal, structural, and hydrogeologic properties spatially and temporally. Technology is available that will allow us to test directly the nature of crustal anisotropy and heterogeneity, the effective

porosity of basement aquifers within which transport of fluids occurs over distances of tens of kilometers, and the continuity (or isolation) of thin regions with the crust separated by only a few meters. Fundamental questions regarding the nature of flow processes within heterogeneous, fractured rock systems can be tested within the seafloor to an extent that is not possible in many aquifer systems on land, because of the consistency and simplicity of boundary conditions and our ability to conduct crustal-scale experiments that last for years and extend for vast distances. On the other hand, there may be basic differences between the hydrogeology of oceanic and continental crustal systems that will be delineated by future studies. Thus marine hydrogeologists must design experiments that will test fundamental assumptions, discriminate between competing conceptual models, and reconcile seemingly contradictory data sets.

References

Abbott, D., Menke, W., Hobart, M., and Anderson, R. 1981. Evidence for excess pore pressures in Southwest Indian Ocean sediments. *J. Geophys. Res.* **86**: 1,813–1,827.

Abbott, D. H., Menke, W., Hobart, M., Anderson, R. N., and Embley, R. W. 1984. Correlated sediment thickness, temperature gradient, and excess pore pressure in a marine fault block basin. *Geophys. Res. Lett.* **11**: 485–488.

Alt, J. C. 1995, Subseafloor processes in mid-ocean ridge hydrothermal systems. In *Seafloor Hydrothermal Systems: Physical, Chemical, Biological and Geological Interactions*, eds. S. E. Humphris, R. A. Zierenberg, L. S. Mullineaux, and R. E. Thompson. Washington, DC: American Geophysical Union, pp. 85–114.

Alt, J. C. and Teagle, D. A. H. 2003. Hydrothermal alteration of upper oceanic crust formed at a fast spreading ridge: mineral, chemical, and isotopic evidence from ODP Site 801. *Chem. Geol.* **201**(3–4): 191–211.

Alt-Epping, P. and Smith, L. 2001. Computing geochemical mass transfer and water/rock ratios in submarine hydrothermal systems: imlications for estimating the vigour of convection. *Geofluids* **1**(3): 163–182.

Anderson, R. N., Hobart, M. A., and Langseth, M. G. 1979. Geothermal convection through oceanic crust and sediments in the Indian Ocean. *Science* **204**: 828–832.

Bach, W., Humphris, S. E., and Fisher, A. T. in press. Fluid flow and fluid–rock interaction within oceanic crust: reconciling geochemical, geological and geophysical observations. In *Subseafloor Biosphere at Mid-ocean Ridges*, eds. C. Cary, E. Delong, D. Kelley, and W. S. D. Wilcock Washington, DC: American Geophysical Union.

Bair, E. S. and Lahm, T. D. 1996. Variations in capture-zone geometry of a partially penetrating pumping well in an unconfined aquifer. *Ground Water* **34**(5): 842–852.

Baker, E. T. 1996. Geological indexes of hydrothermal venting. *J. Geophys. Res.* **101**(B6): 13,741–13,753.

Baker, E. T. and Urabe, T. 1996. Extensive distribution of hydrothermal plumes along the superfast spreading East Pacific Rise, 13° 30′–18° 40′ *S. J. Geophys. Res.* **101**(B4): 8,685–8,695.

Baker, E. T., Chen, Y. J., and Morgan, J. P. 1996. The relationship between near-axes hydrothermal cooling and the spreading rate of mid-ocean ridges. *Earth. Planet. Sci. Lett.* **142**: 137–145.

Baker, P., Stout, P., Kastner, M., and Elderfield, H. 1991. Large-scale lateral advection of seawater through oceanic crust in the central equatorial Pacific. *Earth. Planet. Sci. Lett.* **105**: 522–533.

Barker, P. and Lawver, L. 2000. Anomalous temperatures in central Scotia Sea sediments – bottom water variation or pore water circulation in old crust. *Geophys. Res. Lett.* **27**(1): 13–16.

Beck, A. E., Wang, K., and Shen, P. Y. 1985. Sub-bottom temperature perturbations due to temperature variations at the boundary of inhomogeneous lake or oceanic sediments, *Tectonophysics* **121**: 11–24.

Becker, K., Langseth, M. G., and Hyndman, R. D. 1984. Temperature measurements in Hole 395A, Leg 78B. In *Initial Reports of the Deep Sea Drilling Project*, eds. R. Hyndman and M. Salisbury. Washington, DC: US Govt. Printing Office, pp. 689–698.

Becker, K., Bartetzko, A., and Davis, E. E. 2001. Leg 174B synopsis: revisiting Hole 395A for logging and long-term monitoring of off-axis hydrothermal processes in young oceanic crust. In *Proceedings of the Ocean Drilling Program, Scientific Results*, eds. K. Becker and M. J. Malone. College Station, TX: Ocean Drilling Program, pp. 1–12.

Becker, M. W. and Shapiro, A. M. 2000. Tracer transport in fractured crystalline rock: evidence of nondiffusive breakthrough tailing. *Water Resources Res.* **36**(7): 1,677–1,686.

Becker, N. C., Wheat, C. G., Mottl, M. J., Karsten, J., and Davis, E. E. 2000. A geological and geophysical investigation of Baby Bare, locus of a ridge flank hydrothermal system in the Cascadia Basin. *J. Geophys. Res.* **105**(B10): 23,557–23,568.

Bethke, C. M. and Johnson, T. M. 2002. Paradox of groundwater age. *Geology* **30**(2): 107–110.

Blackman, D. K., Cann, J. R., Janssen, B., and Smith, D. K. 1998. Origin of extensional core complexes: evidence from the Mid-Atlantic Ridge at atlantis fracture zone. *J. Geophys. Res.* **103**(B9): 21,315–21,333.

Bredehoeft, J. D. and Papadopulos, I. S. 1965. Rates of vertical groundwater movement estimated from the earths thermal profile. *Water Resources Res.* **1**: 325–328.

Butterfield, D. A., McDuff, R. E., Mottl, M. J., Lilley, M. D., Lupton, J. E., and Massoth, G. J. 1994. Gradients in the composition of hydrothermal fluids from the Endeavour segment vent field: phase separation and brine loss. *J. Geophys. Res.* **99**: 9,561–9,583.

Butterfield, D. A., Jonasson, I. R., Massoth, G. J., Feely, R. A., Roe, K. K., Embley, R. E., Holden, J. F., McDuff, R. E., Lilley, M. D., and Delaney, J. R. 1997. Seafloor eruptions and evolution of hydrothermal fluid chemistry. *Phil. Trans. Roy. Soc. Lond. A* **355**(1,723): 369–386.

Caine, J. S., Evans, J. P., and Forster, C. B. 1996. Fault zone architechure and permeability structure. *Geology* **24**: 1,025–1,028.

Cann, J. R. 1974. A layered model for oceanic crust developed. *Geophys. J. Roy. Astron. Soc.* **39**: 169–187.

Chen, Y. J. and Phipps Morgan, J. 1996. The effects of spreading rate, the magma budget, and the geometry of magma emplacement on the axial heat flux at mid-ocean ridges. *J. Geophys. Res.* **101**(B5): 11,475–11,482.

Clemo, T. and Smith, L. 1997. A hierarchical approach to simulation of flow and transport in fractured media. *Water Resources Res.* **33**(8): 1,763–1,784.

Converse, D. R., Holland, H. D., and Edmund, J. M. 1980. Flow rates in the axial hot springs of the East Pacific Rise (21° N): implications for the heat budget and the formation of massive sulfide deposits. *Earth. Planet. Sci. Lett*. **69**: 159–175.

Crank, J. 1975, *The Mathematics of Diffusion*. Oxford: Oxford University Press.
Davis, E. E. and Becker, K. 2002. Observations of natural-state fluid pressures and temperatures in young oceanic crust and inferences regarding hydrothermal circulation. *Earth. Planet. Sci. Lett.* **204**: 231–248.
Davis, E. E. and Chapman, D. S. 1996. Problems with imaging cellular hydrothermal convection in oceanic crust. *Geophys. Res. Lett.* **24**: 3,551–3,554.
Davis, E. E. and Fisher, A. T. 1994. On the nature and consequences of hydrothermal circulation in the Middle Valley sedimented rift: inferences from geophysical and geochemical observations, Leg 139. In *Proceedings of the Ocean Drilling Program, Scientific Results*, eds. E. E. Davis, M. J. Mottl., A. T. Fisher, and J. F. Slack. College Station, TX: Ocean Drilling Program, pp. 695–717.
Davis, E. E. and Villinger, H. 1992. Tectonic and thermal structure of the Middle Valley sedimented rift, northern Juan de Fuca Ridge. In *Proceedings of the Ocean Drilling Program, Initial Results*, eds. E. E. Davis, M. Mottl, and A. T. Fisher. College Station, TX: Ocean Drilling Program, pp. 9–41.
Davis, E. E., Chapman, D. S., Mottl, M. J., Bentkowski, W. J., Dadey, K., Forster, C., Harris, R., Nagihara, S., Rohr, K., Wheat, G., and Whiticar, M. 1992. FlankFlux: an experiment to study the nature of hydrothermal circulation in young oceanic crust. *Can. J. Earth Sci.* **29**(5): 925–952.
Davis, E. E., Chapman, D. S., and Forster, C. B. 1996. Observations concerning the vigor of hydrothermal circulation in young volcanic crust. *J. Geophys. Res.* **101**: 2,927–2,942.
Davis, E. E., Wang, K., He, J., Chapman, D. S., Villinger, H., and Rosenberger, A. 1997. An unequivocal case for high Nusselt-number hydrothermal convection in sediment-buried igneous oceanic crust. *Earth. Planet. Sci. Lett.* **146**: 137–150.
Davis, E. E., Chapman, D. S., Wang, K., Villinger, H., Fisher, A. T., Robinson, S. W., Grigel, J., Pribnow, D., Stein, J., and Becker, K. 1999. Regional heat flow variations across the sedimented Juan de Fuca Ridge eastern flank: constraints on lithospheric cooling and lateral hydrothermal heat transport. *J. Geophys. Res.* **104**(B8): 17,675–17,688.
Davis, E. E., Wang, W., Thomson, R. E., Becker, K., and Cassidy, J. F. 2001. An episode of seafloor spreading and associated plate deformation inferred from crustal fluid pressure transients. *J. Geophys. Res.* **106**(B10): 21,953–21,963.
Davis, E. E., Wang, K., Becker, K., Thomson, R. E., and Yashayaev, I. 2003. Deep-ocean temperature variations and implications for errors in seafloor heat flow determinations. *J. Geophys. Res.* **108**(B1): 2,034.
Delaney, J. R., Kelley, D. S., Lilley, M. D., Butterfield, D. A., Baross, J. A., Wilcock, W. S. D., Embley, R. W., and Summit, M. 1998. The quantum event of oceanic crustal accretion: impacts of diking at mid-ocean ridges. *Science* **281**(5374): 222–230.
Delaney, J. R., Robigou, V., McDuff, R., and Tivey, M. 1992. Geology of a vigorous hydrothermal system on the Endeavor segment, Juan de Fuca Ridge. *J. Geophys. Res.* **97**: 19,663–19,682.
Detrick, R. S., Williams, D. L., Mudie, J. D., and Sclater, J. G. 1974. The Galapagos Spreading Centre: bottom-water temperatures and the significance of geothermal heating. *Geophys. J. Roy Astron. Soc.* **38**: 627–636.
Dunn, R. A. and Toomey, D. R. 2001. Crack-induced seismic anisotropy in the oceanic crust across the East Pacific Rise (9° 30′ N). *Earth Planet. Sci. Lett.* **189**: 9–17.
Elder, J. W. 1965, Physical processes in geothermal areas. In ed. W. H. K. Lee, *Terrestrial Heat Flow*. Washington, DC: American Geophysical Union, pp. 211–239.

Elderfield, H. and Schultz, A. 1996. Mid-ocean ridge hydrothermal fluxes and the chemical composition of the ocean. *Ann. Rev. Earth Planet. Sci.* **24**: 191–224.

Elderfield, H., Wheat, C. G., Mottl, M. J., Monnin, C., and Spiro, B. 1999. Fluid and geochemical transport through oceanic crust: a transect across the eastern flank of the Juan de Fuca Ridge. *Earth. Planet. Sci. Lett.* **172**: 151–165.

Fehn, U. and L. Cathles, 1979. Hydrothermal convection at slow-spreading midocean ridges. *Tectonophysics* **55**: 239–260.

1986. The influence of plate movement on the evolution of hydrothermal convection cells in the oceanic crust. *Tectonophysics* **125**: 289–312.

Fehn, U., Green, K., Von Herzen, R. P., and Cathles, L. 1983. Numerical models for the hydrothermal field at the Galapagos Spreading Center. *J. Geophys. Res.* **88**: 1,033–1,048.

2003. Geophysical constraints on hydrothermal circulation: observations and models. In *Energy and Mass Transfer in Submarine Hydrothermal Systems*, eds. P. Halbach, V. Tunnicliffe, and J. Hein. Berlin: Dahlem University Press, pp. 29–52.

Fisher, A. and Becker, K. 2000. Channelized fluid flow in oceanic crust reconciles heat-flow and permeability data. *Nature* **403**: 71–74.

Fisher, A., Giambalvo, E., Sclater, J., Kastner, M., Ransom, B., Weinstein, Y., and Lonsdale, P. 2001. Heat flow, sediment and pore fluid chemistry, and hydrothermal circulation on the east flank of Alarcon Ridge, Gulf of California. *Earth. Planet. Sci. Lett.* **188**: 521–534.

Fisher, A. T. and Becker, K. 1991. Heat flow, hydrothermal circulation and basalt intrusions in the Guaymas Basin, Gulf of California. *Earth. Planet. Sci. Lett.* **103**: 84–99.

1995. The correlation between heat flow and basement relief: observational and numerical examples and implications for upper crustal permeability. *J. Geophys. Res.* **100**: 12,641–12,657.

Fisher, A. T., Becker, K., Narasimhan, T. N., Langseth, M. G., and Mottl, M. J. 1990. Passive, off-axis convection on the southern flank of the Costa Rica Rift. *J. Geophys. Res.* **95**: 9,343–9,370.

Fisher, A. T., Becker, K., and Narasimhan, T. N. 1994. Off-axis hydrothermal circulation: parametric tests of a refined model of processes at Deep Sea Drilling Project/Ocean Drilling Program site 504. *J. Geophys. Res.* **99**: 3,097–3,121.

Fisher, A. T., Davis, E. E., Hutnak, M., Spiess, V., Zühlsdorff, L., Cherkaoui, A., Christiansen, L., Edwards, K. M., Macdonald, R., Villinger, H., Mottl, M. J., Wheat, C. G., and Becker, K. 2003. Hydrothermal recharge and discharge across 50 km guided by seamounts on a young ridge flank. *Nature* **421**: 618–621.

Gelhar, L., Welty, C., and Rehfeldt, K. 1992. A critical review of data on field-scale dispersion in aquifers. *Water Resources Res.* **28**(7): 1,955–1,974.

Geller, G. A., Weissel, J. K., and Anderson, R. N. 1983. Heat transfer and intraplate deformation in the central Indian Ocean. *J. Geophys. Res.* **88**(B2): 1,018–1,032.

Giambalvo, E., Fisher, A. T., Darty, L., Martin, J. T., and Lowell, R. P. 2000. Origin of elevated sediment permeability in a hydrothermal seepage zone, eastern flank of Juan de Fuca Ridge, and implications for transport of fluid and heat. *J. Geophys. Res.* **105**(B1): 913–928.

Giambalvo, E., Steefel, C., Fisher, A., Rosenberg, N., and Wheat, C. G. 2002. Effect of fluid–sediment reaction on hydrothermal fluxes of major elements, eastern flank of the Juan de Fuca Ridge. *Geochim. Cosmochim. Acta* **66**(10): 1,739–1,757.

Goldfarb, M. S. and Delaney, J. R. 1988. Response of two-phase fluids to fracture configurations within submarine hydrothermal systems. *J. Geophys. Res.* **93**: 4,585–4,594.

Goode, D. J. 1996. Direct simulation of groundwater age. *Water Resources Res.* **32**: 289–296.

Green, K. E., Von Hergen, R. P., and Williams, D. L. 1981. The Galapagos spreading center at 86° W: a detailed geothermal field study. *J. Geophys. Res.* **86**: 979–986.

Hartline, B. K. and Lister, C. R. B. 1981. Topographic forcing of super-critical convection in a porous medium such as the oceanic cost. *Earth Planet. Sci. Lett.* **55**: 75–86.

Haymon, R. M. 1996, The response of ridge-crest hydrothermal systems to segmented episodic magma supply. In *Tectonic, Magmatic, Hydrothermal, and Biological Segmentation of Mid-ocean Ridges*, ed. C. L. Walker. Washington, DC: American Geophysical Union, pp. 157–168.

Haymon, R. M., Fornari, D. J., Edwards, M. H., Carbotte, S., Wright, D., and Macdonald, K. C. 1991. Hydrothermal vent distribution along the East Pacific Rise crest (9° 09′−54′ N) and its relationship to magmatic and tectonic processes on fast-spreading mid-ocean ridges. *Earth. Planet. Sci. Lett.* **104**: 513–534.

Hickey, J. J. 1989. An approach to the field study of hydraulic gradients in variable-salinity ground water. *Ground Water* **27**(4): 531–539.

Houtz, R. and Ewing, J. 1976. Upper crustal structure as a function of plate age. *J. Geophys. Res.* **81**: 2,490–2,498.

Huang, P. Y. and Solomon, S. C. 1988. Centroid depths of mid-ocean ridge earthquakes: dependence on spreading rate. *J. Geophys. Res.* **93**: 13,445–13,477.

Hubbert, M. K. 1940. The theory of groundwater motion. *J. Geol.*, **48**: 785–944.

1956. Darcy's law and the field equivalent of the flow of underground fluids. *Trans. Am. Inst. Mining Metal. Eng.* **207**: 222–239.

Humphris, S. E. and Cann, J. R. 2000. Constraints on the energy and chemical balances of the modern TAG and ancient Cyprus seafloor sulfide deposits. *J. Geophys. Res.* **105**(B12): 28,477–28,488.

Ingebritsen, S. E. and Sanford, W. E. 1998. *Groundwater in Geologic Processes*. New York: Cambridge University Press.

Jacobson, R. S. 1992. Impact of crustal evolution on changes of the seismic properties of the uppermost oceanic crust. *Rev. Geophys.* **30**: 23–42.

Johnson, H. P., Hutnak, M., Dziak, R. P., Fox, C. G., Urcuyo, I., Cowen, J. P., Nabelek, J., and Fisher, C. 2000. Earthquake-induced changes in a hydrothermal system on the Juan de Fuca mid-ocean ridge. *Nature* **407**: 174–176.

Kadko, D. and Butterfield, D. A. 1998. The relationship of hydrothermal fluid composition and crustal residence time to maturity of vent fields on the Juan de Fuca Ridge. *Geochim. Cosmochim. Acta* **62**(9): 1,521–1,533.

Kadko, D. and Moore, W. 1988. Radiochemical constraints on the crustal residence time of submarine hydrothermal fluids: Endeavour Ridge. *Geochim. Cosmochim. Acta* **52**: 659–668.

Karson, J. A. 1998. Internal structure of oceanic lithosphere: a perspective from tectonic windows. In *Faulting and Magmatism at Mid-ocean Ridges*, eds. W. R. Buck, P. T. Delaney, J. A. Karson, and Y. Lagabrielle, Washington, DC: American Geophysical Union, pp. 177–218.

2002. Geologic structure of the uppermost oceanic crust created at fast- to intermediate-rate spreading centers. *Ann. Rev. Earth Planet. Sci.* **30**: 347–384.

Karson, J. A. and Rona, P. A. 1990. Block-tilting, transfer faults, and structural control of magmatic and hydrothermal processes in the TAG area, mid-Atlantic 26° North. *Geol. Soc. Am. Bull.* **102**: 1,635–1,645.

Kelley, D. S., Delaney, J. R., and Yoerger, D. R. 2001. Geology and venting dynamics of the Mothra hydrothermal field, Endeavour Segment, Juan de Fuca Ridge. *Geology* **29**(10): 959–962.

Kimura, S., Schubert, G., and Straus, J. M. 1986. Route to chaos in porous-medium thermal convection. *J. Fluid Mech.* **166**: 305–324.

Kleinrock, M. C. and Humphris, S. E. 1996. Structural control on sea-floor hydrothermal activity at the TAG active mound. *Nature* **382**: 149–153.

Klitgord, K. D. and Mudie, J. D. 1974. The Galapagos Spreading Center: a near-bottom geophysical study. *Geophys. J. Roy Astron. Soc.* **26**: 623–626.

Kong, L. S. L., Solomon, S. C., and Purdy, G. M. 1992. Microearthquake characteristics of a mid-ocean ridge along-axis high. *J. Geophys. Res.* **97**(B2): 1,659–1,685.

Langseth, M. G. and Herman, B. 1981. Heat transfer in the oceanic crust of the Brazil Basin. *J. Geophys. Res.* **86**: 10,805–10,819.

Langseth, M. G., Hyndman, R. D., Becker, K., Hickman, S. H., and Salisbury, M. H. 1984. The hydrogeological regime of isolated sediment ponds in mid-oceanic ridges. In *Initial Reports of the Deep Sea Drilling Project*, eds. R. H. Hyndman and M. H. Salisbury. Washington, DC: US Govt. Printing Office, pp. 825–837.

Langseth, M. G., Mottl, M. J., Hobart, M. A. and Fisher, A. T. 1988. The distribution of geothermal and geochemical gradients near site 501/504: implications for hydrothermal circulation in the oceanic crust. In *Proceedings of the Ocean Drilling Program, Initial Reports*, Vol. 111, eds. K. Beaker, H. Sakai, *et al.* College Station, TX: Ocean Drilling Program, pp. 23–32.

Langseth, M. G., Becker, K., Von Herzen, R. P., and Schultheiss, P. 1992. Heat and fluid flux through sediment on the western flank of the Mid-Atlantic Ridge: a hydrogeological study of North Pond. *Geophys. Res. Lett.* **19**: 517–520.

Lapwood, E. 1948. Convection of a fluid in a porous media. *Proc. Camb. Phil. Soc.* **44**: 508–521.

Larson, R. L., Fisher, A. T., and Jarrard, R. 1993. Highly layered and permeable Jurassic oceanic crust in the western Pacific. *Earth. Planet. Sci. Lett.* **119**: 71–83.

Lilley, M. D., Butterfield, D. A., Olson, E. J., Lupton, J. E., Macko, S. A., and McDuff, R. E. 1993. Anomalous CH4 and $NH4^+$ concentrations at an unsedimented mid-ocean ridge hydrothermal system. *Nature* **364**(6432): 45–47.

Lister, C. R. B. 1972. On the thermal balance of a mid-ocean ridge. *Geophys. J. Roy Astron. Soc.* **26**: 515–535.

Lu, N. and Ge, S. 1996. Effect of horizontal heat and fluid flow on the vertical temperature distribution in a semiconfining layer. *Water Resources Res.* **32**(5): 1,449–1,453.

Macdonald, K. C., Fox, P. J., Alexander, R. T., Pockalny, R., and Gente, P. 1996. Volcanic growth faults and the origin of Pacific abyssal hills. *Nature* **380**: 125–129.

Matthews, M., Salisbury, M., and Hyndman, R. 1984. Basement logging on the Mid-Atlantic Ridge, Deep Sea Drilling Project Hole 395A. In *Initial Reports of the Deep Sea Drilling Project*, eds. R. D. Hyndman and M. H. Salisbury. Washington, DC: US Govt. Printing Office, pp. 717–730.

Mayer, L., Theyer, F., *et al.* 1985. Site 571. *Initial Reports of the Deep Sea Drilling Project*, Vol. 85, eds. L. Mayer, F. Theyer, *et al.* Washington, DC: US Govt. Printing Office, pp. 23–32.

McDuff, R. E. 1981. Major cation gradients in DSDP interstitial waters: the role of diffusive exchange between seawater and upper oceanic crust. *Geochim. Cosmochim. Acta* **45**: 1,705–1,713.

Moores, E. M. and Vine, F. J. 1971. The Troodos massif, Cyprus, and other ophiolites as oceanic crust: evaluations and implications. *Phil. Trans. Roy. Soc. Lond. Series A* **268**: 443–466.

Moreno, L. and Tsang, C.-F. 1994. Flow channeling in strongly heterogeneous porous media: a numerical study. *Water Resources Res.* **30**: 1,421–1,430.

Mottl, M. J. 1989. Hydrothermal convection, reaction and diffusion in sediments on the Costa Rica Rift flank, pore water evidence from ODP Sites 677 and 678. In *Proceedings of the Ocean Drilling Program, Scientific Results*, Vol. 111, eds. K. Becker and H. Sakai. College Station, TX: Ocean Drilling Program, pp. 195–214.

Mottl, M. J. and Wheat, C. G. 1994. Hydrothermal circulation through mid-ocean ridge flanks: fluxes of heat and magnesium. *Geochim. Cosmochim. Acta* **58**: 2,225–2,237.

Mottl, M. J., Wheat, C. G., Baker, E., Becker, N., Davis, E., Feeley, R., Grehan, A., Kadko, D., Lilley, M., Massoth, G., Moyer, C., and Sansone, F. 1998. Warm springs discovered on 3.5 Ma oceanic crust, eastern flank of the Juan de Fuca Ridge. *Geology* **26**: 51–54.

Murton, B. J., Redbourn, L. J., German, C. G., and Baker, E. T. 1999. Sources and fluxes of hydrothermal heat, chemicals and biology within a segment of the Mid-Atlantic Ridge. *Earth. Planet. Sci. Lett.* **171**: 301–317.

Neuman, S. P. 1990. Universal scaling of hydraulic conductivities and dispersivities in geologic media. *Water Resources Res.* **26**(8): 1,749–1,758.

Nield, D. A. 1968. Onset of thermohaline convection in a porous medium. *Water Resources Res.* **4**: 553–560.

Oberlander, P. L. 1989. Fluid density and gravitational variations in deep boreholes and their effect on fluid potential. *Ground Water* **27**(3): 341–350.

Park, J., Bethke, C. M., Torgersen, T., and Johnson, T. M. 2002. Transport modeling applied to the interpretation of groundwater 36Cl age. *Water Resources Res.* **38**: 1–15.

Parsons, B. and Sclater, J. G. 1977. An analysis of the variation of ocean floor bathymetry and heat flow with age. *J. Geophys. Res.* **82**: 803–829.

Phipps Morgan, J. and Chen, Y. J. 1993. The genesis of oceanic crust: magma injection, hydrothermal circulation, and crustal flow. *J. Geophys. Res.* **98**: 6,283–6,297.

Purdy, M. and Detrick, R. 1986. Crustal structure of the Mid-Atlantic Ridge at 23° N from seismic refraction studies. *J. Geophys. Res.* **91**: 3,739–3,762.

Purdy, M., Kong, L. S. L., Christeson, G. L., and Solomon, S. C. 1992. Relation between spreading rate and the seismic structure of mid-ocean ridges. *Nature* **355**: 815–817.

Raitt, R. W. 1963, The crustal rocks. In *The Sea*. ed. M. N. Hill, New York: Wiley-Interscience, pp. 85–102.

Ribando, R., Torrence, K., and Turcotte, D. 1976. Numerical models for hydrothermal circulation in the oceanic crust. *J. Geophys. Res.* **81**: 3,007–3,012.

Rosenberg, N., Fisher, A., and Stein, J. 2000. Large-scale lateral heat and fluid transport in the seafloor: revisiting the well-mixed aquifer model. *Earth. Planet. Sci. Lett.* **182**: 93–101.

Sanford, W. E. 1997. Correcting for diffusion in Carbon-14 dating of ground water. *Ground Water* **35**(2): 357–361.

Schultz, A., Delaney, J. R., and McDuff, R. E. 1992. On the partitioning of heat flux between diffuse and point source seafloor venting. *J. Geophys. Res.* **97**: 12,299–12,315.

Sclater, J. G. and Francheteau, J. 1970. The implications of terrestrial heat flow observations on current tectonic and geochemical models of the crust and upper mantle of the earth. *Geophys. J. Roy. Astron. Soc.* **20**: 509–542.

Sclater, J. G., Von Herzen, R. P., Williams, D. L., Anderson, R. N., and Klitgord, K. 1974. The Galapagos Spreading Center: heat flow on the north flank. *Geophys. J. Roy. Astron. Soc.* **38**: 609–626.

Shapiro, A. M. 2001. Effective matrix diffusion in kilometer-scale transport in fractured rock. *Water Resources Res.* **37**(3): 507–522.

Shapiro, A. M. and Hsieh, P. A. 1998. How good are estimates of transmissivity from slug tests in fractured rocks? *Ground Water* **36**(1): 37–48.

Sleep, N. and Wolery, T. 1978. Egress of hot water from mid-ocean ridge hydrothermal systems, some thermal constraints. *J. Geophys. Res.* **83**: 5,913–5,922.

Smith, D. K. and Cann, J. R. 1993. Building the crust at the Mid-Atlantic Ridge. *Nature* **365**: 707–715.

1999. Constructing the upper crust of the Mid-Atlantic Ridge: a reinterpretation based on the Puna Ridge, Kilauea Volcano. *J. Geophys. Res.* **104**: 25,379–25,399.

Snelgrove, S. H. and Forster, C. B. 1996. Impact of seafloor sediment permeability and thickness on off-axis hydrothermal circulation: Juan de Fuca Ridge eastern flank. *J. Geophys. Res.* **101**: 2,915–2,925.

Sohn, R. A., Webb, S. C., Hildebrand, J. A., and Cornuelle, B. C. 1997. Three-dimensional tomographic velocity structure of upper crust, CoAxial segment, Juan de Fuca Ridge: implications for on-axis evolution and hydrothermal circulation. *J. Geophys. Res.* **102**: 17,679–17,695.

Spinellic, G. A. and Fisher, A T. in Press. Hydrothermal circulation within rough basement on the Juan is Fuca Ridge Flank. *Geochem. Geophys. Geosys*.

Stein, J. S. and Fisher, A. T. 2001. Multiple scales of hydrothermal circulation in Middle Valley, northern Juan de Fuca Ridge: physical constraints and geologic models. *J. Geophys. Res.* **106**(B5): 8,563–8,580.

2003. Observations and models of lateral hydrothermal circulation on a young ridge flank: reconciling thermal, numerical and chemical constraints. *Geochem. Geophys. Geosys*. doi:10.1029/200290000415.

Stephen, R. 1981. Seismic anisotropy observed upper oceanic crust. *Geophys. Res. Lett.* **8**: 865–868.

Stephen, R. A. 1985. Seismic anisotropy in the upper oceanic crust. *J. Geophys. Res.* **90**: 11,383–11,396.

Sudicky, E. A. and Frind, E. O. 1981. Carbon 14 dating of groundwater in confined aquifers: implications of aquitard diffusion. *Water Resources Res.* **17**(4): 1,060–1,064.

Travis, B. J., Janecky, D. R., and Rosenberg, N. D. 1991. Three-dimensional simulation of hydrothermal circulation at mid-ocean ridges. *Geophys. Res. Lett.* **18**: 1,441–1,444.

Tsang, C.-F. and Tsang, Y. W. 1989. Flow channeling in a single fracture as a two-dimensional strongly heterogeneous permeable medium. *Water Resources Res.* **25**(9): 2,076–2,080.

Tsang, C. F. and Neretnieks, I. 1998. Flow channeling in heterogeneous fractured rocks. *Rev. Geophys.* **36**(2): 275–298.

Tsang, C.-F., Tsang, Y. W., and Hale, F. V. 1991. Tracer transport in fractures: analysis of field data based on a variable-aperature channel model. *Water Resources Res.* **27**(12): 3,095–3,106.

Villinger, H., Grevemeyer, I., Kaul, N., Hauschild, J., and Pfender, M. 2002. Hydrothermal heat flux through aged oceanic crust: where does the heat escape? *Earth Planet. Sci. Lett.* **202**(1): 159–170.

Von Damm, K. L. 1995. Controls on the chemistry and temporal variability of seafloor hydrothermal fluids. In *Seafloor Hydrothermal Systems: Physical, Chemical, Biological and Geological Interactions*, eds. S. E. Humphris, R. A. Zierenberg, L. S. Mullineaux, and R. E. Thompson, Washington, DC: American Geophysical Union, pp. 222–247.

Von Herzen, R., Ruppel, C., Molnar, P., Nettles, M., Nagihara, S., and Ekstrom, G. 2001. A constraint on the shear stress at the Pacific–Australian plate boundary from heat flow and seismicity at the Kermadec Forearc. *J. Geophys. Res.* **106**(B4): 6,817–6,833.

Wang, K., He, J., and Davis, E. E. 1997. Influence of basement topography on hydrothermal circulation in sediment-buried oceanic crust. *Earth Planet. Sci. Lett.* **146**: 151–164.

Wheat, C. G. and McDuff, R. 1994. Hydrothermal flow through the Mariana Mounds: dissolution of amorphous silica and degredation of organic mater on a mid-ocean ridge flank. *Geochim. Cosmochim. Acta* **58**: 2,461–2,475.

Wheat, C. G., Elderfield, H., Mottl, M. J., and Monnin, C. 2000. Chemical composition of basement fluids within an oceanic ridge flank: implications for along-strike and across-strike hydrothermal circulation. *J. Geophys. Res.* **105**(B6): 13,437–13,447.

Wheat, C. G. and Mottl, M. J. 1994. Hydrothermal circulation, Juan de Fuca Ridge eastern flank: factors controlling basement water composition. *J. Geophys. Res.* **99**: 3,067–3,080.

Wilcock, W. S. D. and Fisher, A. T. in press. Geophysical constraints on the sub-seafloor environment near mid-ocean ridges. In *Subseafloor Biosphere at Mid-ocean Ridges*, eds. C. Cary, E. Delong, D. Kelley, and W. S. D. Wilcock. Washington, DC: American Geophysical Union.

Wilcock, W. S. D. and McNabb, A. 1996. Estimates of crustal permeability on the Endeavour segment of the Juan de Fuca mid-ocean ridge. *Earth Planet. Sci. Lett.* **138**: 83–91.

Williams, D. L., Von Herzen, R. P., Sclater, J. G., and Anderson, R. N. 1974. The Galapagos Spreading Centre, lithospheric cooling and hydrothermal circulation. *Geophys. J. Roy. Astron. Soc.* **38**: 587–608.

Wooding, R. A. 1960. Instability of a viscous liquid of variable density in a vertical Hele-Shaw cell. *J. Fluid Mech.* **7**: 501–515.

Wright, D. J., Haymon, R. M., and Macdonald, K. C. 1995. Breaking new ground: estimates of crack depth along the axial zone of the East Pacific Rise ($9^\circ 12' - 54'$ N). *Earth Planet. Sci. Lett.* **134**: 441–457.